Study of Resonant Charge Transfer

by

Edward E. Rickman, Jr.

Thesis submitted to the Faculty of the
Virginia Polytechnic Institute and State University in
partial fulfillment of the requirements for the degree of

Master of Science

in

Chemistry

APPROVED:

G. Sanzone, Chairman

Raymond E. Dessy

Paul E. Field

John G. Mason

John C. Schug

March, 1985

Blacksburg, Virginia

STUDY OF RESONANT CHARGE TRANSFER

by

Edward E. Rickman, Jr.

Committee Chairman: George Sanzone

Chemistry

(ABSTRACT)

Experimental measurements of N_2 resonant charge transfer cross sections were performed. It was found that the energy of electrons used to produce the N_2^+ ions is an important variable with respect to cross section. An examination of the experimental precision was performed and it was found that the precision of measurement was insufficient to determine the exact form of this relationship. The effect of ion energy (collisional energy) was too small to be seen.

Modulated detection was used to improve precision and permit measurement at high noise levels. A description of the apparatus is provided. Consideration

of other systems (O_2, NO, and CO) and the suitability of their resonant charge transfer reactions for experimental investigation is discussed. Various theoretical models for estimation of cross section were examined.

Acknowledgements

I would like to thank my wife Diane for her support, understanding, and assistance in the preparation of this work. I would like to express my gratitude to Dr. George Sanzone for his guidance and assistance, to James Browder for his assistance and technical support, and to R. Rover for logistical support. I would also like to thank Dr. Alphonsa Smith for his support. Additionally, I would like to thank my committee members, Drs. R. E. Dessy, P. E. Field, J. G. Mason, and J. C. Schug, for their patience and support.

Table of Contents

Table of Figures

Table of Tables

Now you know that the answer to the ultimate question of life, the universe, and everything is forty two. All you need to do now is find out what the question is.

Donald Adams[1]

I. INTRODUCTION

One of the most important goals of physical chemistry is the correlation of the quantum mechanical states of species with chemical reactivity. Charge transfer reactions are a class of reactions well suited to both experimental and theoretical study of the reactivity of quantum states. Experimentally, the studies are simplified by the use of electrical and magnetic fields to focus, mass select, and energy select both reactant and product ions. One simple means for the production of ionized molecules is by electron bombardment *i. e.*:

(1) $$A(v=0, \varphi) + e^- \rightarrow A^+(v=n, \varphi^*) + 2e^-.$$

Unfortunately, the energy variation in practical electron beams precludes selection of rotational or vibrational states (although in some systems slight control of the vibrational state distribution can be obtained). However, the electronic states of the ion beam can be manipulated by control of the electron accelerating energy. This control allows the production of ion beams with varying ratios of ground and excited states, which permits examination of the effects of excited electronic states on reactivity.

One of the goals of this work was to examine the of the electron energy used in ion-beam production on reactivity in charge transfer reactions. Many past experimental works have been done with unspecified electron energies. If the electron energy is a major influence on reactivity, then proper control of the electron energy will be necessary both for examination of experimental trends and for comparison of experimental data to theoretical models. Another goal was to develop measures of the precision of the cross sections obtained. This is necessary for comparison both to experimental models and to measurements made in other laboratories.

Before considering criteria for the selection of systems, it is useful to discuss some of the terminology employed in the study of charge transfer reactions. All reactions considered will involve the transfer of a single electron from a neutral molecule to a positive ion: *i. e.*,

$$A^+ + B \xrightarrow{\Delta E} A + B^+ \quad . \tag{2}$$

If the two species differ only by the presence or absence of an electron (*e. g.* N_2^+ and N_2, or Ar^+ and Ar), then the

reaction is said to be a *symmetric* charge transfer reaction. Here, the reaction produces no net change in species (although the microscopic states involved may change). If the net energy change is zero then the reaction is said to be *resonant*. This is satisfied in the symmetric case when there is no net difference in the quantum states of reactant and product. Resonant charge transfer may also occur if other states of the combined products have the same energy as the reactants. This may also occur in assymmetric charge transfer; for example, certain states of N_2^+ are resonant with Ar as was seen in studies of the following system:[2]

(3) $$Ar^+ + N_2 \rightarrow N_2^+ + Ar \ .$$

Because cross sections are greater (at the energies used in this experiment) in the resonant case, resonant cross sections are easier to measure experimentally. For this reason, only resonant systems were considered. Since symmetric reactions always have a resonant reaction path, these reactions are most suitable for study. Criteria for the selection of reactions as well as examination of possible candidates are discussed in the next section.

II. HISTORICAL AND THEORETICAL REVIEW

II A. SYSTEM SELECTION

To probe the effect of excited electronic states on reactivity, it was necessary that the reaction selected for study satisfy certain criteria. First, to simplify ion production and detection, the system should be gaseous at low pressures (*i. e.* $P \leq 10^{-3}$Torr) and room temperatures. It was also desirable that the species chosen be neither corrosive nor oxidizing (this reduces problems due to burnt-out filaments and surface dirt). Second, the system should exhibit no major side reactions (*e. g.* atom exchange, dissociation, *etc.*) under the conditions of study. Third, the ground and at least one excited state of the ion must have sufficient lifetimes to survive transport to the reaction cell (greater than 4μsec at about 500 eV). Since the state population of the ion beam will be varied by the energy of the ionizing electron beam, the ground and excited states should be separated by as much energy as possible. Fourth, in order to insure large cross sections, the vibrational and electronic states of the ion and neutral should have maximum overlap (See section on impact parameter cross section

calculations). Fifth, theoretical calculations should exist for comparison with experimental results.

One of the first systems to be considered was the symmetric nitric oxide (NO) reaction. The ion's ground state ($X^1\Sigma^+$) occurs[3] at 9.27eV while the first two excited states[3] (according to photoelectron spectroscopy), $b^3\pi$ and $A^1\pi$, occur at 16.55 and 18.32 eV respectively. The ground state is stable while the $A^1\pi$ and $b^3\pi$ states have lifetimes of 56ns and 160μs respectively.[4] Unfortunately, there are a large number of states which are not accessable by photon bombardment and thus both their energy levels and potentials are in dispute.[3] For this reason, NO was not further considered as a test system.

A second system considered was nitrogen (N_2). Here, the ground state and two excited states are readily accessible. The ground state ($X^2\Sigma_g^+$) occurs[5] at 15.63eV. The first excited state $A^2\pi u$ occurs[5] at 17.0eV and has a lifetime[6] between 12.28μs (v=1) and 9.14μs (v=5). The second excited state ($B^2\Sigma_u^+$) occurs at[5] 18.94eV and has a reported lifetime[6,7] between 66ns to 80ns, decaying to the ($X^2\Sigma_g^+$) ground state. As this lifetime is shorter than the ion transit time ($\approx$ 4μsec), the $B^2\Sigma_u^+$ state will not be

seen. However, the $A^2\pi_u$ state, having a lifetime greater than the transit time, will be seen in the ion beam. The fraction of ground state ($X^2\Sigma_g^+$) in the ion beam will decline above the ionization potential of the first excited state ($A^2\pi_u$), due to production of $A^2\pi\mu$ ions. As the electron energy is further increased, the fractions of both the ground ($X^2\Sigma_g^+$) and first excited ($A^2\pi_u$) states should decline as the second ($B^2\Sigma_u^+$) state is produced. However, since the $B^2\Sigma_g^+$ state decays to the ground state, the net fraction of ground state should begin to increase for electron energies above the ionization potential of the second ($B^2\Sigma_u^+$) state. Thus, the net effect of varying electron energy should be a dip in the percentage of the ground state at electron energies slightly above the energy of the first excited state ($A^2\pi_u$). This enables the ratios of excited states in the ion beam to be varied and their effect on reactivity studied. An examination of vibrational overlap (Figure 1) shows that the ground ionic state ($X^2\Sigma_g^+$) has good overlap with the ground neutral state while the excited ($A^2\pi_u$) state has much poorer vibrational overlap with the ground neutral state.[8] Calculations of charge transfer cross section by the impact parameter method indicate a much lower cross section for the $A^2\pi_u$ state than for the ground $X^2\Sigma_g^+$ state

due to this poorer vibrational overlap.[9] Experimental work of Flannery *et. al.*[9] indicates a dip in cross section near 35eV electron energy for ion energy at 733 eV. This dip in cross section is about 8% below calculated impact parameter calculations and has been attributed to the $A^2\pi_u$ state.[9] At higher ion energies, this discrepancy is not seen.[9] Experimental measurements were made in an attempt to reproduce this dip. As the current apparatus should be capable of lower ion energies than the above work, it would be interesting to see if the dip is more prominent at even lower ion energies.

Another interesting system is CO which is isoelectronic with N_2. Here the same term symbols apply (without the + and g symmetry) but at different energies. The CO ground state ($X^2\Sigma$) has an energy[11] of 14.01 eV and is stable. The first excited state ($A^2\pi$) has an energy[11] of 16.58eV and lifetimes from 3.5μs (v=1) to 2.4μs (v=6) decaying to the $X^2\Sigma$ (ground) state.[10] The second excited state $B^2\Sigma$ has an energy[9] of 19.70eV and a lifetime of 45nsec, decaying to the ground ($X^2\Sigma$) state.[12] At an electron energy of 46.5eV, the $A^2\pi$ state represents about 55% of the ion beam with the remainder in the $X^2\Sigma$ ground state.[10] Since the lifetime of the $A^2\pi$ state is on the

order of the transit time of the instrument, it should be possible to vary its concentration by varying the ion transit time. With the magnetic mass spectrometer used, this may be accomplished by varying the ion energy while compensating with the magnetic field; *i. e.*

$$m/q = kB^2/V, \tag{4}$$

where m/q is the mass to charge ratio, B is the magnetic induction, V is the ion-accelerating voltage, and k is a constant for the specific mass spectrometer in use. Since the ion-beam energy at the reaction cell can be controlled separately by the voltage applied to the cell, it should be possible to perform cross-section measurements at a fixed ion energy but with different ion-transit times (and thus different $A^2\pi$ concentrations), thus directly probing the effect of the excited state.

The last system which was considered was the O_2^+ - O_2 resonant charge exchange[13]. The ground ($X^2\pi_g$) state has an energy of 12.09 (eV). The first excited state ($a^4\pi_\mu$) has an energy of 16.1eV and a lifetime in excess of 20μsec. The second excited state ($A^2\pi\mu$) has an energy of

16.8eV and decays to the ground state. The third excited state ($b^4\Sigma_g^-$) state occurs at 18.2eV and decays to the $a^4\pi_\mu$ state. It is expected that only the ground ($X^2\pi_g$) and $a^4\pi_\mu$ states will be seen in the ion beam.[4,14] The fraction of $a^4\pi_\mu$ state in an ion beam produced by electrom bombardment was found to be 22% at 25eV, 30% at 50eV, and 33% at 100eV electron energies.[14] Examination of potential curves for both ion and neutral (Figure 2)[8] indicates that the $a^4\pi_\mu$ state of the ion has better vibrational overlap with the ground ($X^3\Sigma_g^-$) neutral state and should thus have a larger cross section than the ground ($X^2\pi_\mu$) state (See section on impact parameter calculations). Because both states receive contributions from decaying states above them, there should be no sharp variation in concentration except at the $a^4\pi_\mu$ ionization potential. Because this is about 16eV, it is difficult to get substantial ion production in this region, making the difference between the states hard to experimentally probe.

After consideration of these four systems, it was decided that the $N_2^+ - N^2$ system should be investigated first, as it has well-studied electronic states that have provided for the prediction of cross section data.[9] In

addition, preliminary data indicated that a difference in excited state reactivity exists.[9]

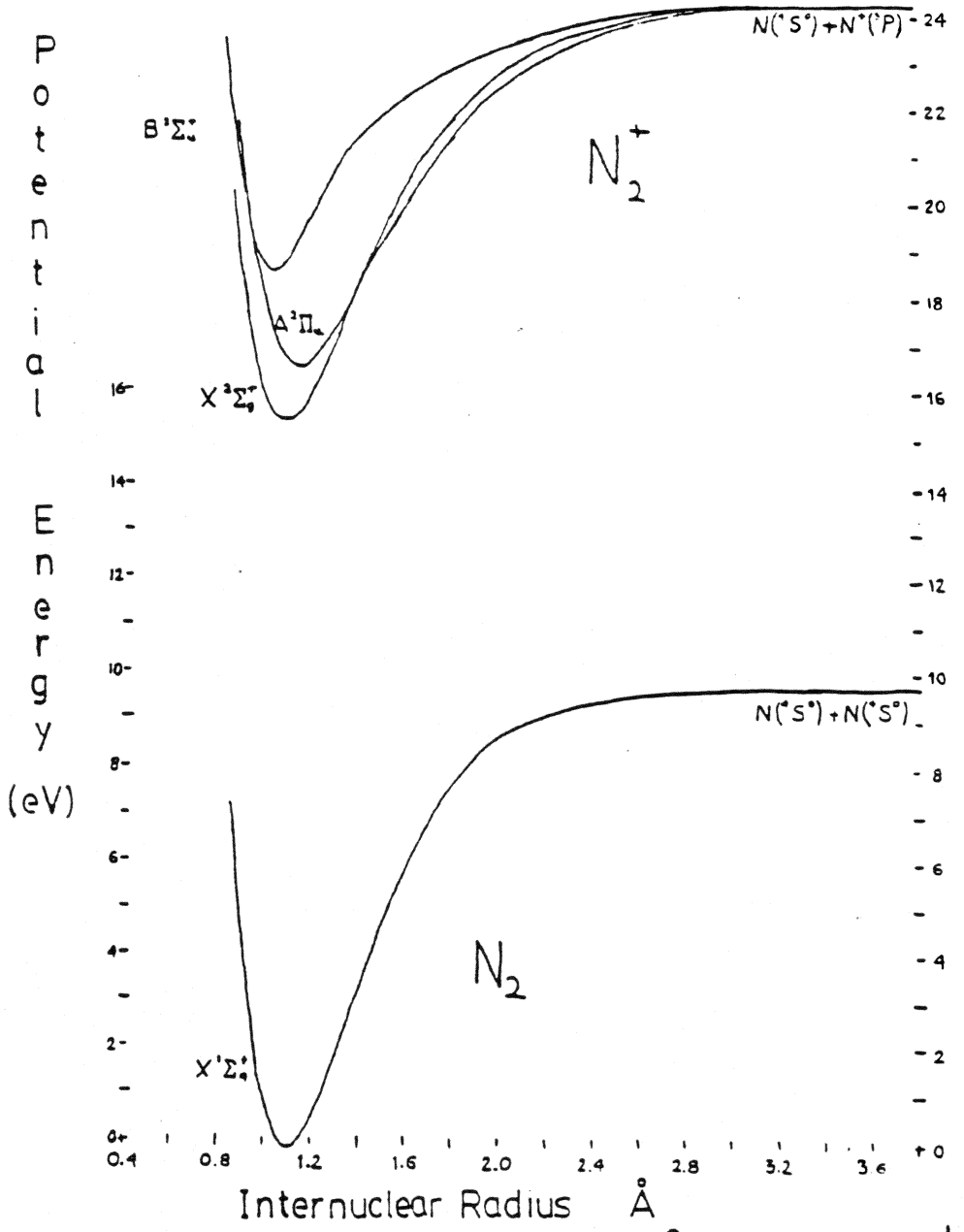

Figure 1-Potential Curves[8] of N_2 and N_2^+

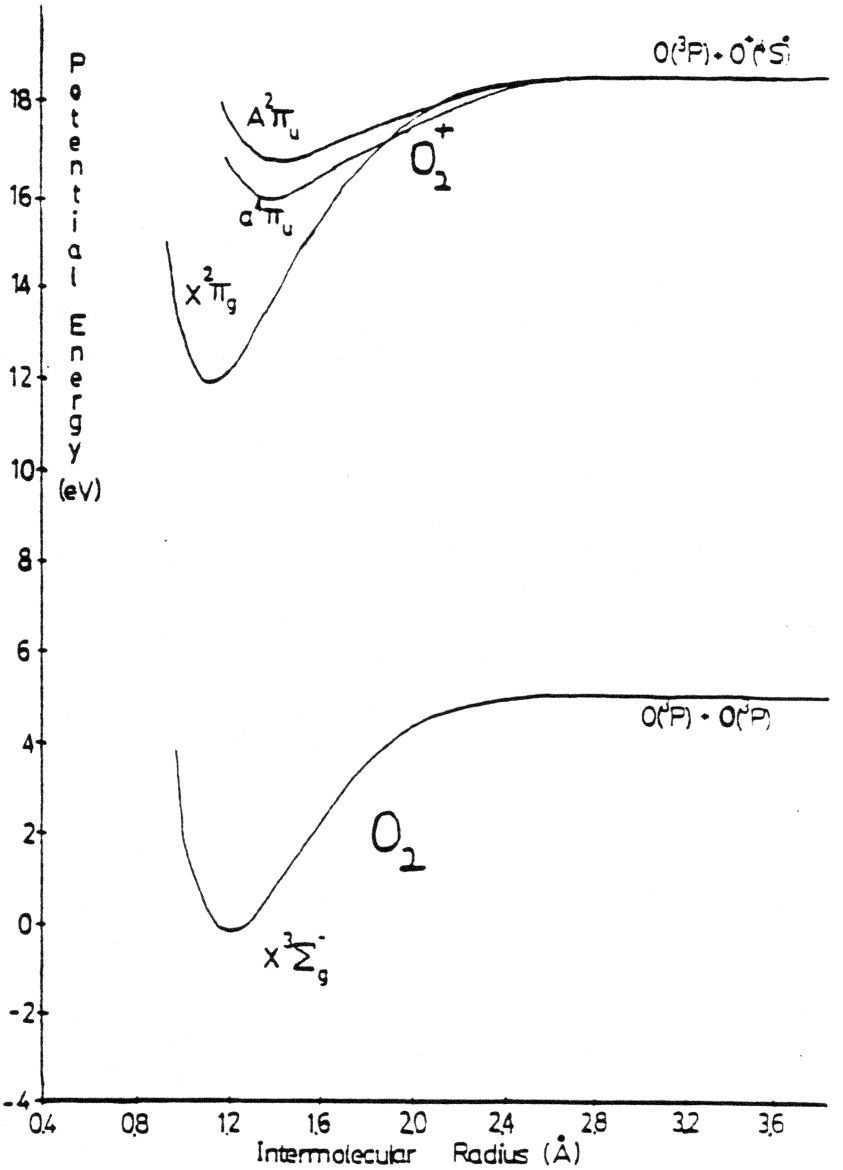

Figure 2 - Potential Curves[8] for O_2 and O_2

II B. CROSS SECTION

In studies of kinetics by molecular beam techniques, the cross section is typically used as a measure of the rate of reaction. For a beam impinging on a target, the change in beam current due to collision (ΔI) is,

$$\Delta I = -I_o \rho = -I_o \frac{\text{Area}_{\text{Target}}}{\text{Area}_{\text{Beam}}}$$

where I_o is the incident beam intensity and ρ is the collision probability. With a thin gaseous target,

$$A_{\text{Target}} = N\, A_{\text{Beam}}\, \Delta x\, \sigma \tag{6}$$

where N is the number density of the gas (molecules/unit volume), Δx is the path length and σ is the cross section or effective area of each molecule. Here, a thin target is defined as one of sufficiently low density that no molecule shadows another (*i. e.* no molecule is in front of another). Upon substuting equation 6 into equation 5, the following is obtained:

$$\frac{-\Delta I}{I_o} = n\, \Delta x\, \sigma\ . \tag{7}$$

In the limit of infintesimal path length ($\Delta x \to 0$) this yields

(8) $$\frac{dI}{I} = N \sigma \, dx$$

or,

(9) $$\frac{\partial \ln I}{\partial x} = N \sigma \, .$$

Integrating over the cell length x (and assuming N and σ are constant), gives

(10) $$\ln\left[\frac{I_x}{I_o}\right] = \sigma N x,$$

where I_x is the beam intensity at the end of the cell. For charge transfer

(11) $$I_x = I_o - I_{CT},$$

where I_{CT} is the current of molecules produced by charge transfer (See the section on reaction cell). Ideal gas behavior is assumed (*i. e.* $N = \frac{P}{kT}$, where P is the reaction

cell pressure, k is the Boltzmann constant, and T is the absolute temperature). Then,

$$\left[1 - \frac{I_{CT}}{I_o}\right] = \frac{\sigma P x}{kT} \tag{12}$$

or,

$$\sigma = \frac{kT}{Px} \ln\left[1 - \frac{I_{CT}}{I_o}\right] . \tag{13}$$

This equation permits the experimental measurement of cross section.

It should be noted that the cross section is a function of collision velocity ($v\rightarrow$) *i. e.*,

$$\sigma = \sigma(v\rightarrow) \tag{14}$$

With this in mind, cross sections can be related to the bimolecular thermal reaction rate constant, which is more usually employed in chemical studies. For the reaction,

$$A + B \rightarrow C + D \tag{15}$$

the rate constant [k(T)] is given by

(16) $$k(T) = \frac{dN_B}{N_B\ N_A\ dt}\ .$$

Upon substituting equation 8, the following is obtained:

(17) $$k(\upsilon\rightarrow) = \frac{N_A\ \sigma(\upsilon\rightarrow)\ dx}{N_A\ \ dt}$$

or,

(18) $$k(\upsilon\rightarrow) = \sigma\ (\upsilon\rightarrow)\ \upsilon\rightarrow.$$

But since k represents an average over a temperature distribution of velocities, the expectation value of k must be taken; *i. e.*,

(19) $$k(T) = \langle k(\upsilon\rightarrow)\ \rangle = \int_{-\infty}^{\infty} \sigma(\upsilon\rightarrow)\ \rho(\upsilon\rightarrow,T)\ \upsilon\rightarrow\ d\upsilon\rightarrow$$

where $\rho(\upsilon\rightarrow,T)$ is the distribution of velocities at temperature T (typically a Boltzmann distribution is used).

II C. CLASSICAL CHARGE TRANSFER CALCULATIONS

The basic model for the classical ion-molecule cross section is the Langevin model.[15] The system is considered to be composed of point particles, where one particle is fixed and the other is moving relative to it. The moving particle approaches with a velocity $v\rightarrow$ and is off axis by a distance (called the impact parameter) b (See Figure 3). An attractive potential field V(r) exists between the particles. At b=0, all collisions result in capture (and it is assumed that reaction occurs). But for b>0, the incoming particle has rotational energy and thus experiences a centrifugal repulsive force. For a given initial velocity, the magnitude of the centrifugal force increases with b. Thus, for any initial velocity there is a maximum (or critical) value of $b = b_c$ that permits orbiting capture. The capture cross section is given by the area of the circle with radius equal to $b_c(v\rightarrow)$; *i. e.*,

$$\sigma(v\rightarrow) = \pi\,[b_c(v\rightarrow)]^2. \qquad (20)$$

For an ion-neutral reaction (such as charge transfer) the attractive potential is due to ion-induced

dipole interaction; *i. e.*,

$$(21) \qquad V(r) = \int_r^\infty F(r)dr = \int_r^\infty \frac{\alpha q^2 dr}{2\pi\varepsilon_o r^5} = -\frac{\alpha q^2}{8\pi\varepsilon_o r^4}$$

where α is the polarizability, q is the charge, r is the intermolecular radius and ε_o is the permittivity of free space. The rotational potential energy is:

$$(22) \qquad E_{rot} = \frac{L^2}{2\mu r^2} = \frac{\mu v_\rightarrow^2 b^2}{2r^2}$$

where L is the angular momentum and μ is the reduced mass. The total effective potential is the sum of the attractive potential and the repulsive centrifugal potential, *i. e.*:

$$(23) \qquad V_{eff}(r) = -\frac{\alpha q^2}{8\pi\varepsilon_o r^4} + \frac{\mu^2 v_\rightarrow^2 b^2}{2r^2}.$$

For the critical impact parameter $b = b_c(v_\rightarrow)$, the incoming species has just sufficient energy to orbit the target; *i. e.*, the relative energy (E_r) is equal to the potential

energy (no translational energy occurs) or;

$$(24) \qquad V_{eff}(r)\Big|_{b=b_c} = \frac{L^2}{2\mu r^2} - \frac{\alpha q^2}{8\pi\varepsilon_o r^4} = E_r .$$

Also, at the critical radius ($r = r_c(v\rightarrow)$) where the orbiting collision occurs (for $b = b_c(v\rightarrow)$) the effective potential has a maximum:

$$(25) \qquad \frac{\partial V(r)}{\partial r}\Big|_{r=r_c} = 0 = \frac{L^2}{\mu r_c^3} + \frac{\alpha q^2}{2\pi\varepsilon_o r_c^5} .$$

Equations 24 and 25 provide two simultaneous equations in the variables $b_c(v\rightarrow)$ and $r_c(v\rightarrow)$. Solution gives,[15]

$$(26) \qquad b_c = \left[\frac{\alpha q^2}{2\pi\varepsilon_o E_r}\right]^{1/4}$$

and thus,

$$(27) \qquad \sigma(v) = \pi b_c^2 = q\left[\frac{\pi\alpha}{2\varepsilon_o E_r}\right]^{1/2} .$$

In more convenient units, this is,

$$\sigma(E) = 5.33 \left[\frac{\alpha}{E_r}\right]^{1/2} \quad (\text{Å}^2), \tag{28}$$

where α is in $cm^3 * 10^{25}$ and E is in eV. A table of polarizability values for some common species is provided as Table 1.[21]

Various attempts have been made to extend the Langevin theory to ion-polar molecule reactions. Typically, the rates of protron and other atom transfer reactions have been studied. One of the first attempts (referred to as the "locked rotor" approach) to include the dipole effect was done by Moran and Hamill.[15,19] Here, at low collision velocities it was assumed that the dipole was aligned with the molecular collision axis. Introducing the dipole moment into the potential function, the determination of cross section was performed similarly to the Langevin (induced dipole) cross section. At higher velocities, the Langevin cross section was used on the grounds that orientation of the dipole is no longer possible. At intermediate velocities, a weighted average of the two (*i. e.* dipole and induced dipole) cross

sections was used.[17] This approach tends to overestimate the effect of the ion-dipole interaction, resulting in cross sections larger than the experimental values. This provides an upper theoretical bound.[15]

A second method (due to Dugan and Magee[15,20]) was to solve the classical equations for a rotating dipole under the influence of an ionic molecule. Initial positions and orientations were chosen at random. As in the Langevin case, the capture cross section was calculated. It was found that orbiting collisions did not occur unless the minimum radius was below some critical value (typically 1-2Å).[20] This simpler criterion was then used to evaluate whether a given trajectory led to capture.[15,20] It was also found that the capture cross section varied with respect to the $-0.6^{\underline{th}}$ to $-0.7^{\underline{th}}$ power of the translational energy; *i. e.* ,

$$\sigma(E) = cE^{-n} \tag{29}$$

where E is the translational energy, c is a constant and n is between -0.6 and -0.7.[22] This last assumption doesn't allow for a variable rate of dipole "locking" in different

species that can produce spurious cross sections.[15]

A third approach is due to Su and Bowers.[15] Here, the method is similar to the locked dipole approach of Moran and Hamill,[19] but assumes the dipole locks at some average angle with respect to the ion. This angle is calculated at the critical radius r_c (as in the Langevin method) as the expectation value over a distribution that includes the effects of the rotational energy as well as the number of ways a given molecule can be oriented with a given angle θ. This average angle θ is then used (as in the locked rotor approach) to calculate a capture cross section.[15] A variation of this method[23] is to calculate the variation of cross section with angle, and then to calculate the expectation value of the cross section over the angular distribution. The first approach tends to work better in the limit of non-polar reactions, while the second approach works better in the limit of polar molecules.[15]

In examining the above capture methods with respect to charge transfer, four things should be noted. First, such cross sections only consider the orbiting capture under the influence of long-range forces.[16]

Second, it must be assumed that every capture results in charge exchange (or else that some fixed efficiency exists).[16] Third, where reactions other than charge transfer exist, the total cross section must be divided among these reactions.[17] If ion or atom transfer reactions are exothermic, then these will predominate at the expense of charge transfer.[17] Indeed, it is for this class of reaction that the Langevin cross sections are most sucessful. Fourth, charge transfer reactions generally show less dependence of cross section on kinetic energy, as can be seen by examination of Table 2. An equation of the following form is typically used to extrapolate data for charge transfer reactions,

$$\sigma^{1/2} = -k_1 \ln v\rightarrow + k_2, \tag{30}$$

where k_1 and k_2 are fitted constants and $v\rightarrow$ is the relative velocity.[17] The difference in energy dependence between charge transfer and capture cross sections suggests that an orbiting collision is not necessary for charge transfer, otherwise the experimental values for charge transfer cross sections should decline much more rapidly at high kinetic energies. Thus the capture cross sections are less suitable for charge transfer than the impact parameter methods (to be discussed later).

TABLE 1 - MOLECULAR POLARIZABILITIES (α) [21]

Molecule	$\alpha * 10^{25}$ (cm^3)
H^2	7.9
N_2	17.6
O_2	16.0
CO_2	19.5
N_2O	30.0
CH_4	26.0
Cl_2	46.1
CCl_4	105

TABLE 2 - CROSS SECTION DATA FOR $N_2^+ + N_2 = N_2 + N_2^+$

Kinetic energy (lab eV)	Experimental cross section[18] ($Å^2$)	Langevin cross section[21] ($Å^2$)
1	39.1	22.4
3	36.1	12.9
5	28.1	10.0
10	23.1	7.1
20	22.7	5.0
50	21.7	3.2

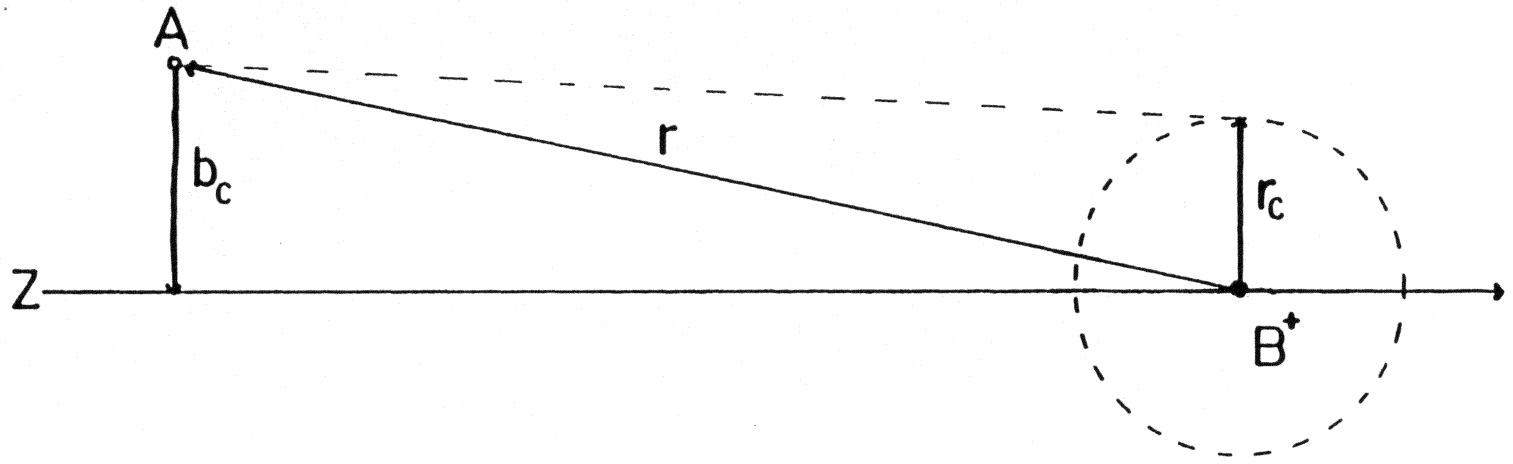

Figure 3 - Langevin Orbiting Collision

II D. IMPACT PARAMETER CROSS SECTION CALCULATIONS

The "impact parameter" method is a semi-classical method of charge transfer calculations in which the velocity and impact parameter are well defined (usually fixed). This limits the velocities to below 10^8cm/sec,[27] which corresponds to about 70keV for $N_2^+ - N_2$ or $CO^+ - CO$ collisions. At low energies, the basic assumptions are that the wavelengths associated with the momentum and with the momentum transfer must be small compared to the impact parameter.[24] The use of a fixed velocity and impact parameter limits the minimum applicable velocity to approximately $(10^5/\mu^{1/2})$ cm/sec (i. e. $\approx 5*10^{-3}$eV for $N_2^+ - N_2$ or $CO^+ - CO$) where μ is the reduced mass, in Daltons.[27] This is due to a failure to allow for curved trajectories under the influence of the intermolecular potential. The time-dependent Schrodinger equation is solved by a perturbation treatment using the interaction between the ion and neutral as the perturbation. The probabilities of charge transfer, calculated at each impact parameter are integrated over all impact parameters and over all phase space to give the cross section:[24]

$$\sigma = 2\pi\int_0^\infty P(b)\ b\ db, \tag{31}$$

where b is the impact parameter and P(b) is the probability of reaction at a given impact parameter. Two approaches have been used in formulating the system's description. The first (referred to as the "atomic" case by Flannery[9]) describes the system in terms of the wave functions of the ion and neutral at infinite separation. The initial (or direct) state is given by the wave functions of A and B^+ evaluated at infinite separation. The final (or exchange) state is given by the wave functions of A^+ and B, also evaluated at infinite seperation. The wave function of the total system is taken as the sum of the initial and final states.[24] The time dependent Schrödinger equation may be written as:[24]

$$(32) \quad c_i H' \psi_i + c_f H' \psi_f = i\frac{h}{2\pi}\frac{\partial}{\partial t}(c_i \psi_i + c_f \psi_f)$$

where c_i and c_f are the coefficients of the initial and final states, ψ_i and ψ_f are the initial and final wave functions, H' is the perturbed Hamiltonian, and h is Planck's constant. The Schrödinger equation is solved (as above) and the phase shift is taken into the coefficients[9,24] *i. e.*:

$$(33) \quad C = ce^{iw}$$

where C is the new coefficient, c is the amplitude, and w is the phase. The probability of charge transfer (and thus the cross section by equation 31) is given by the complex product of the coefficients of the final state:[24]

(34) $$P(b) = c_f^{*}\, c_f \Big|_{x \to \infty}$$

One problem occurs in the asymmetric case; microscopic reversability may be violated. The cross section for the reaction:

(35) $$A + B^{+} \rightarrow A^{+} + B$$

should be the same as the cross section for the reverse reaction:

(36) $$A^{+} + B \rightarrow A + B^{+},$$

since the reactions differ only in the sign of the relative velocity vector.[25] However, in the first reaction wave functions made from A and B^{+} were used while in the second reaction wave functions made from A^{+} and B were used. Thus the transition probabilities need not be

equal. This can be avoided by including product Hamiltonium terms, which can be ignored in the symmetric case. Often, however, these terms are difficult to evaluate and thus ignored in the hope that they are sufficiently small.[24]

The second case (referred to by Flannery as the "molecular" case)[9] involves the formation of wave functions for the $(A...B)^+$ complex. These wave functions are usually chosen as one-electron wave functions about the A^+ and B^+ cores. The time-dependent Schroedinger equation is solved to obtain the cross sections.

So far, the vibrational terms have been neglected. If they are assumed to be separable then a vibrational overlap term can be added to the wave functions:[26]

(37) $$\Psi = \Psi_{el}\ \Psi_{vib}.$$

The coefficients of the wavefunctions are the product of three terms; the first, a ground state electronic term, the second a vibrational energy term, and the third, a phase shift associated with the time dependent equation

i. e.:

(38) $$C = c\ P(l,m)e^{iw}$$

where C is the coefficient, c is the electronic coefficient, P(l,m) is a vibrational overlap term, and the exponential is associated with the time dependent solution. The cross sections may then be thought of as being the product of two terms, a vibrational overlap (Franck-Condon) term and an electronic probability term. Thus, charge transfer occurs most efficiently when both the energies of product and reactant states are the same and when the internuclear radii of both A and B are unchanged in the reaction process.

For the symmetric case using molecular wave functions,[9] the charge transfer occurs not by an electronic transition (as in the asymmetric case) but by the phase shift produced in the collision. The probability of transfer is given by:[9]

(39) $$P(b) = \sin^2\eta(b)$$

where P(b) is the probability of charge transfer, η is the

phase shift, and b is the impact parameter.

The magnitude of this phase shift is related to splitting of states into gerade and ungerade states by the intermolecular potential; *i. e.*,

$$\eta = \left[\frac{2\pi}{vh}\right] \int_0^\infty [E_g(R) - E_u(R)]dZ \qquad (40)$$

where E_g and E_u are the gerade and ungerade energies respectively, Z is the molecular collision axis, v is the velocity along the Z axis, and h is Planck's constant.[9] This energy difference is related to the interaction potential.[24] Therefore, some measure of the interaction potential is needed to obtain the cross section. For the (H_2^+,H_2) reaction, Bates and Reid[26] calculated this splitting by direct solution of a one-electron wave function around two rigid cores. However, this becomes more difficult for species of higher atomic number. For the (N_2^+, N_2) and (CO^+, CO) systems, Flannery *et. al.*[9] fitted experimental scattering potentials (*i. e.* Lennard - Jones) to a Morse function to obtain the energies needed in equation (39). They obtained the necessary vibrational overlaps from the

literature for v = 0 (for the neutral reactant), and with a Morse potential for higher vibrational states of the neutral. Strictly speaking, these calculations should be done for reactions leading to all allowed product vibrational states. However, since at low velocities the cross section is much greater for resonant (or near resonant) reaction paths, only these paths need be included in calculations. This approach is called the "low-velocity" approximation by Flannery[9]. Furthermore, if both reactants are in their ground vibrational states, then only the products in their ground vibrational states need be considered. This is called a "two-state" approximation.[9] The results of the "low-velocity" calculations are presented in Table 3 for (N_2^+, N_2) and in Table 4 for (CO^+, CO). The agreement between the "low-velocity" and the full multistate calculations are obviously best for moderate energies and low vibrational states. At higher collision energies, increasing contributions from non-resonant reactions must be considered. Calculations including all states with change in vibrational states equal to 0, 1, and 2 are presented for (N_2^+, N_2) in Table 3 and for (CO^+, CO) in Table 4. For the (CO^+, CO) reaction[9] the low-velocity calculations show excellent agreement at energies as high as 733eV and good

agreement as high as 1910eV. The better agreement in the CO reaction is due to the preferential Franck-Condon factors (*i. e.* the radii of CO and CO^+ are more similar than $N_2^+ - N_2$).[9]

Similar calculations have been performed for the $O_2^+ - O_2$ and $NO^+ - NO$ systems.[4] Because vibrational coupling is weaker for resonant channels and stronger for non resonant channels, the two state approximation is not as useful as for the $N_2^+ - N_2$ and $CO^+ - CO$ systems.[4] In the $O_2^+ - O_2$ system, the $a^4\pi\mu$ state (although it decays rapidly) weights the vibrational distribution of the ground state such that a large number of terms are needed for convergence in the multi-state calculation.[4] For this reason, Moran, *et. al.*[30] limited their calculations below the $a^4\pi_u$ ionization potential (16.1eV). In the NO case, the lack of information on ion states that are accessable by electron bombardment (and perhaps by charge transfer) but not by photoionization, makes attempts at experimental verification difficult.[4]

Because of the importance of the vibrational overlap in symmetric resonant charge transfer, it is possible to determine the cross section between any given

reactant and product vibrational states relative to any other set of reactant and product vibrational state (assuming that the same electronic states exist in both sets of reactions).[28] This is a consequence of the assumed separability of electronic and vibrational states. A scaling term (S) can then be defined, *i. e.*,[28]

$$(41) \quad \sigma(v_i', v_i'' \rightarrow v_k', v_l'' | E) = S\, \sigma(v_o', v_o'' \rightarrow v_o', v_o'' | E)$$

where the ' and " represent neutral and ion, respectively, and E is the relative translational energy. This scaling term is simply the ratio of the vibrational overlaps of the desired channel and the reference (v'=0, v"=0) channel multiplied by the ratios of phase shifts in the desired and reference reaction channels. This approach has been used to fit a scaling matrix to the product cross sections:[28,29]

$$(42) \quad \sigma(v_o') = M\, \sigma(0,0 \rightarrow 0,0 | E),$$

where M is a scaling matrix in terms of the scaling parameters (t^2) and f_1. These fitted parameters were then used to deconvolute the state-to-state cross sections. The validity of this approach has been demonstrated[4,28]

by deconvoluting the theoretical product cross sections of Moran, *et. al.*[9] to obtain the theoretical state-to-state cross sections (also of Moran, *et. al.*[9]). Although this does not at first glance seem to be impressive, it should be noted that no assumptions as to the form of the potential were made and only the overlap factors need be known.[28,29] Unfortunately, most experimental data does not readily provide product state distributions suitable for use in this method. However, when and if experimentalists are able to provide such data, this technique may be able to provide state-to-state cross section data.

TABLE 3

Impact Parameter Cross Sections[9] for

$$N_2^+(X^2\Sigma_g^+,\ v_o') + N_2(X^1\Sigma_g^+,\ v_o'=0) \rightarrow N_2(X^1\Sigma_g^+,\ S_{v''}) + N_2^+(X^2\Sigma_g^+,\ S_{v'})$$

v_o'	Method	Ion Energy			
		156eV	400eV	733eV	2210eV
0	low-velocity	36.24	41.30	32.88	14.87
	multistate	36.73	38.70	31.38	15.81
1	low-velocity	38.30	39.10	29.70	12.94
	multistate	35.79	36.73	27.72	14.90
2	low-velocity	39.93	35.80	25.83	10.80
	multistate	33.54	35.03	26.68	13.92
3	low-velocity	39.99	31.49	21.72	8.76
	multistate	30.07	31.67	23.91	12.82
4	low-velocity	37.86	26.45	17.52	6.84
	multistate	25.28	27.37	21.17	11.80
5	low-velocity	33.37	21.01	13.44	5.10
	multistate	20.72	24.23	19.15	10.90
	low-velocity	26.99	15.60	9.70	3.59
	multistate	17.76	22.29	17.94	10.16

TABLE 4

Impact Parameter Cross Sections[9] for

$CO^+(X^2\Sigma^+, v_o') + CO(X^1\Sigma^+, v_o''=0) \rightarrow$

$CO(X^1\Sigma^+, S_{v''}) + CO^+(X^2\Sigma^+, S_{v'})$

v_o'	Method	Ion Energy			
		156eV	400eV	733eV	1910eV
0	low-velocity	33.38	40.55	38.36	22.69
	multistate	32.96	38.81	36.78	22.86
1	low-velocity	33.34	40.80	37.39	21.52
	multistate	33.49	39.40	36.19	22.20
2	low-velocity	33.50	40.87	36.42	20.47
	multistate	33.43	41.37	36.44	22.05
3	low-velocity	33.79	40.79	35.47	19.54
	multistate	33.52	41.68	35.90	21.65
4	low-velocity	34.15	40.62	34.58	18.72
	multistate	33.85	41.60	35.28	21.31
5	low-velocity	34.50	40.42	33.78	18.00
	multistate	34.17	41.40	34.69	21.01
6	low-velocity	34.89	40.15	33.04	17.40
	multistate	34.48	41.15	34.18	20.76

When the only tool you have is a hammer,

every problem begins to look like a nail.

Abram Maslow[31]

III. INSTRUMENTAL

III A. Introduction

The basic design and construction of the apparatus was due to A. Smith.[32] His original apparatus was built and used[32] at the NASA Langley Research Center. In 1980 this apparatus was dismantled and the ion source (without power supply), ion optics, charge transfer cell, and vacuum chamber were sent here to Virginia Tech. It was necessary to supply the following: vacuum systems for the ion source and cell chamber, inlet systems for the ion source and charge transfer cell, power supplies for the ion source and ion optics, and detection facilities for reactant and product ions. Additionally, attempts were made to improve the signal-to-noise ratio by use of a modulated beam detection system. The experimental apparatus (Figure 4) may be described in the following manner. Ions are produced by electron bombardment. The desired ion is then selected on the basis of its mass to charge ratio by passage through a magnetic field. Focusing optics are used to transport the mass selected ions to the reaction cell. At the reaction cell, the

neutral gas, which is maintained at a known pressure, reacts with the ion beam to produce product ions. Energy selection is used to separate the product (slow) ions from scattered and incident (fast) ions. The experimental apparatus can be conveniently broken into four major subsystems:

1) ion production and selection (m/s).

2) ion transport (ion optics).

3) reaction cell and chamber.

4) ion detection.

These are briefly described below in separate sections.

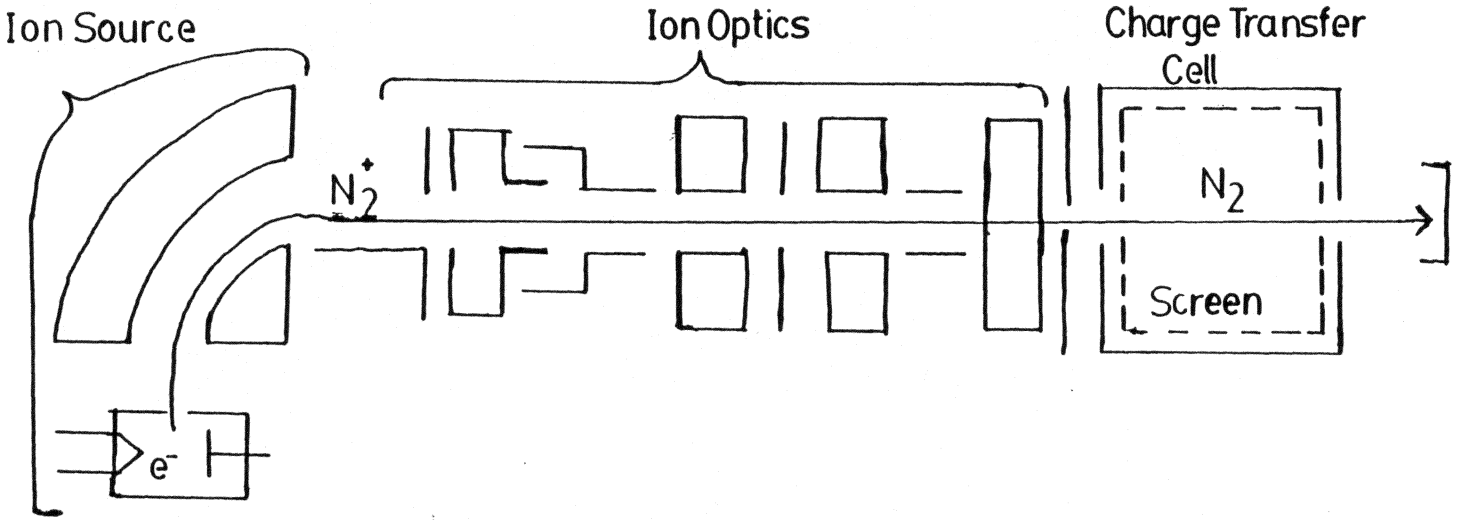

Figure 4 - Charge Transfer Apparatus (not to scale)

III B. 1) Ion Production and Selection

Ions were produced by electron bombardment and the desired species were mass selected in a modified magnetic mass spectrometer (Consolidated Engineering Corporation model 21-401, *circa* 1953).[33] This is a single focusing permanent magnet unit, whose magnetic field is adjustable by motor-driven magnetic shunts. The vacuum system was adapted from a Bendix time-of-flight mass spectrometer and consists of a mercury diffusion pump with refrigerated (Freon TM) trap and liquid nitrogen trap. A bellows valve was installed between the trap and ion source to reduce contamination caused by the boil off of nitrogen trap contents after shutdown. A basic electrical outline of the ion source is given as Figure 5. Originally, a separate electron shield supply was used in an attempt to hold the shield at a potential relative to the filament. It was found that maximum electron-beam current was obtained at zero shield voltage (relative to the filament). Additionally, negative potentials tended to attract the hot filament to the shield, welding and usually breaking the filament. For these reasons the shield was fixed at zero potential. Typical operating potentials are given in Table 5. A rhenium filament was

used with a d.c. heating current of 3.5 A which corresponds to an applied voltage of about 3.3V. A d.c. power supply was used to reduce fluctuation caused by the a.c. electrical supply. The filament was maintained at a positive potential with respect to the ionization chamber by use of a d.c. power supply (Fluke model 407D). This potential is the nominal electron energy. The actual electron energy is affected by the potential gradient across the ionization chamber (necessary to draw ions out of the ionization chamber), by surface charging, and by the potential drop across the surface of the filament. It is necessary to determine experimentally the actual energy of the electron beam in the region of ionization. This is done by determining the appearance potential of N_2^+ (*i. e.* electron-accelerating voltage at which N_2^+ ion current appears). A plot of ion current versus electron potential is made and a straight line is drawn tangent to the rising portion of the curve (see Figure 6). The difference between this voltage and the known appearance potential for N_2^+ (15.75eV) is added as an offset to the nominal electron energy. *i. e.*:

$$(43)\quad eE_{True} = eE_{nominal} + (AP_{True} - AP_{Experimental}).$$

The assumption that a simple offset provided correction was verified by testing mixtures of N_2 and Ar. The offset for N_2^+ yielded correct appearance potentials for Ar^+ and Ar^{2+}. The offset is expected to vary whenever ion-repeller potentials were changed and thus a new offset must be determined. Typically, the offset was determined with each day's run. As such corrections were not systematically applied to previous work with this instrument,[32] this causes doubt as to the validity of the reported electron energies in earlier work.

Ions, produced by electron bombardment, are accelerated across the ionization chamber under the influence of the repeller's potential. The ions are then accelerated by the ion-energy power supply (Kepco model ABC-1000). As in the case of the electron energy, the actual ion energy is determined not only by the selected potential of the ion energy power supply but also by the values of the repeller potentials as well as the charging of ion source surfaces. For this reason, it was necessary to determine the actual ion energy experimentally. This was done by plotting the ion current versus the potential applied to the charge-transfer cell (and screen). The ion energy was defined as the potential at which the ion beam

intensity has been reduced by one half, relative to that at zero potential (See Figure 7). Since the cell (and screen) are maintained at a potential relative to ground (See the section on the reaction cell.), the ion energy during the charge-transfer experiment is given by

(44) $$\text{Ion Energy} = \varphi_{1/2} - \varphi_{CTCS}$$

where $\varphi_{1/2}$ is the retarding potential at half-beam intensity and φ_{CTCS} is the potential applied to the cell. The value of $\varphi_{1/2}$ must be redetermined whenever the repeller voltages or ion-energy potential have been changed. Typically, this was done at the end of each day's run.

The ion-accelerating energy and the magnetic field intensity were varied jointly to achieve the maximum N_2^+ ion current. The magnetic field intensity was varied by changing the distance between two magnetic shunts. Best results were obtained with a shunt gap (distance between shunts) of 1.570cm (0.618in) and an ion-acceleration voltage of about 630V (actual values depend on repeller settings). With an ion-source pressure of about $5.7*10^{-6}$Torr (as measured at the ionization

gauge), a N_2^+ current of $5.3*10^{-9}$A was obtained at the output of the mass spectrometer. This is similar to levels obtained by A. Smith.[32]

A study of ion-source pressure (Figure 8) versus output current shows that a fall off in N_2^+ ion beam current occurs at pressures above $1.0*10^{-6}$Torr. This is likely due to ion-molecule reactions occuring inside the ion source. To avoid this and to maximize the ion current, operating pressure was kept below $8*10^{-6}$Torr. In order to provide for a controlled introduction of gas into the cell, an inlet system (Figure 9) was constructed. Gas was admitted to the manifold at about 200Torr and then expanded into the expansion tank. The resulting pressure was on the order of 500mTorr. The needle valve was adjusted to produce a pressure in the ion source ranging from 4 to $6*10^{-6}$Torr. The use of a preliminary expansion and a needle valve, in addition to the porous frit, allowed the ion-source pressure to be adjusted (and readjusted, if necessary, over long runs) to within 10%. This type of precision is almost impossible to achieve with a needle valve and a "high pressure" (*i. e.* Torr) manifold. A porous frit without the needle valve provides a fixed gas flow which can not be adjusted to allow for

depletion of the manifold. (In principle, a less-porous frit could have been used which would have allowed higher pressures and thus little depletion, but the frit employed was supplied with the ion source and its replacement would have been more difficult than construction of the system actually employed.)

Since the gases employed are of relatively low molecular mass, it was not considered necessary to perform extensive tests of resolution. An indication of the actual resolution is the voltage width of the ion beam. For a magnetic instrument,

(45) $$\frac{m}{q} = \frac{k}{V}$$

where k is an instrument constant (for a fixed magnetic field), V is the ion energy and m/q is the mass to charge ratio. Defining the resolution (R) as

(46) $$R \equiv \frac{m}{\Delta m},$$

and substituting equasion 45, the following is obtained

(47) $$R = \frac{V_L V_H}{V_m(V_H - V_L)} \approx \frac{V}{\Delta V} ;$$

where the subscripts L and H refer to the lower and higher half heights, while the m refers to the midpoint of the peak. For nitrogen (N_2^+), with an ion voltage of 692V and a half width of about 5V, this gives a resolution of about 138, which is more than adequate for these studies.

TABLE 5

Typical Ion Source Parameters for N_2^+

(see Figure 5 for definition of voltages)

element	voltage (V)
electron energy	70.0
inner repeller	69.3
outer repeller	31.4
inner focus	44.6
outer focus	47.3
anode	19.5
ion energy	629

Temp. ≈ 390^{0}F.

Heater current ≈ 2.5A.

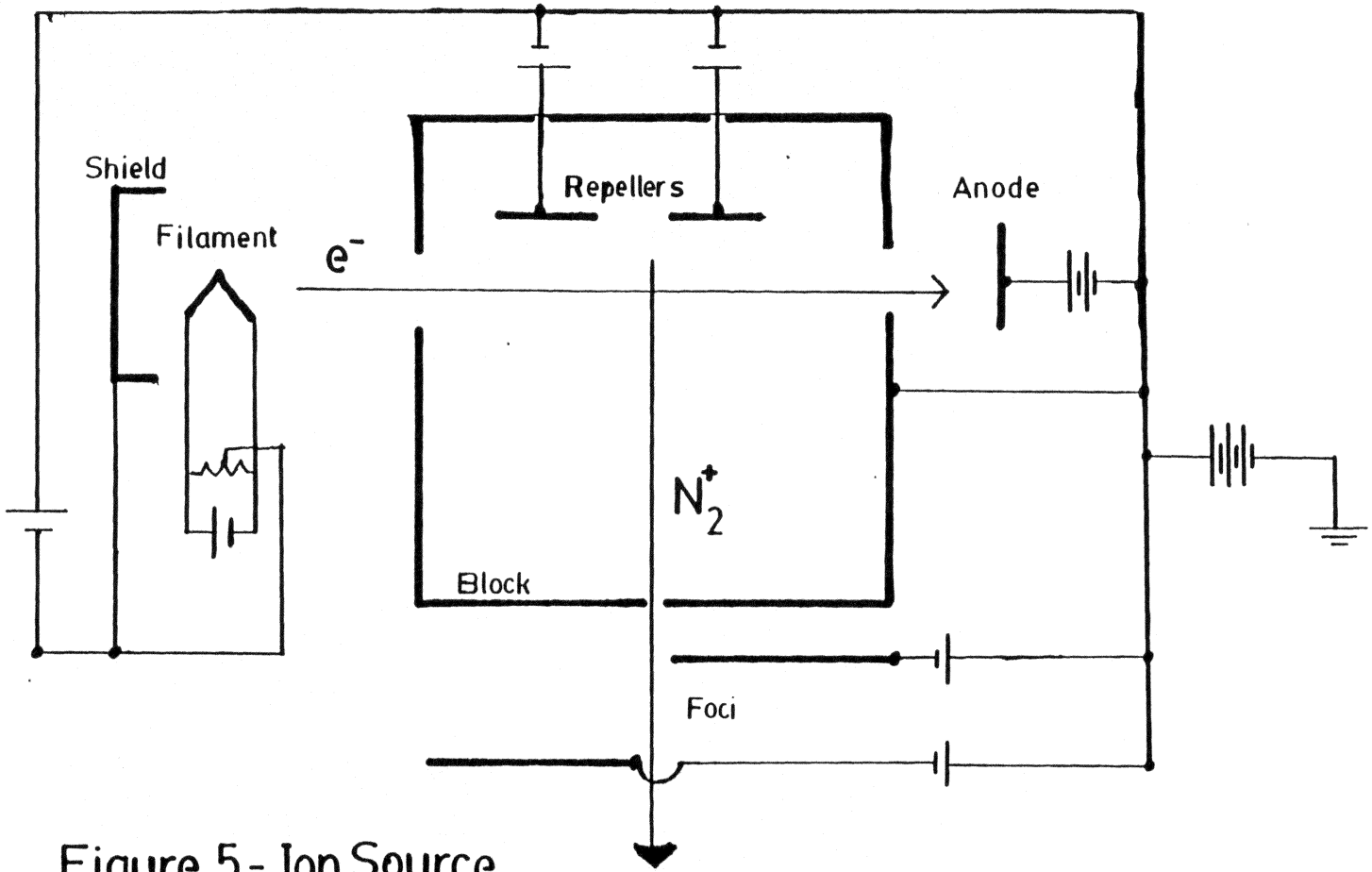

Figure 5 - Ion Source

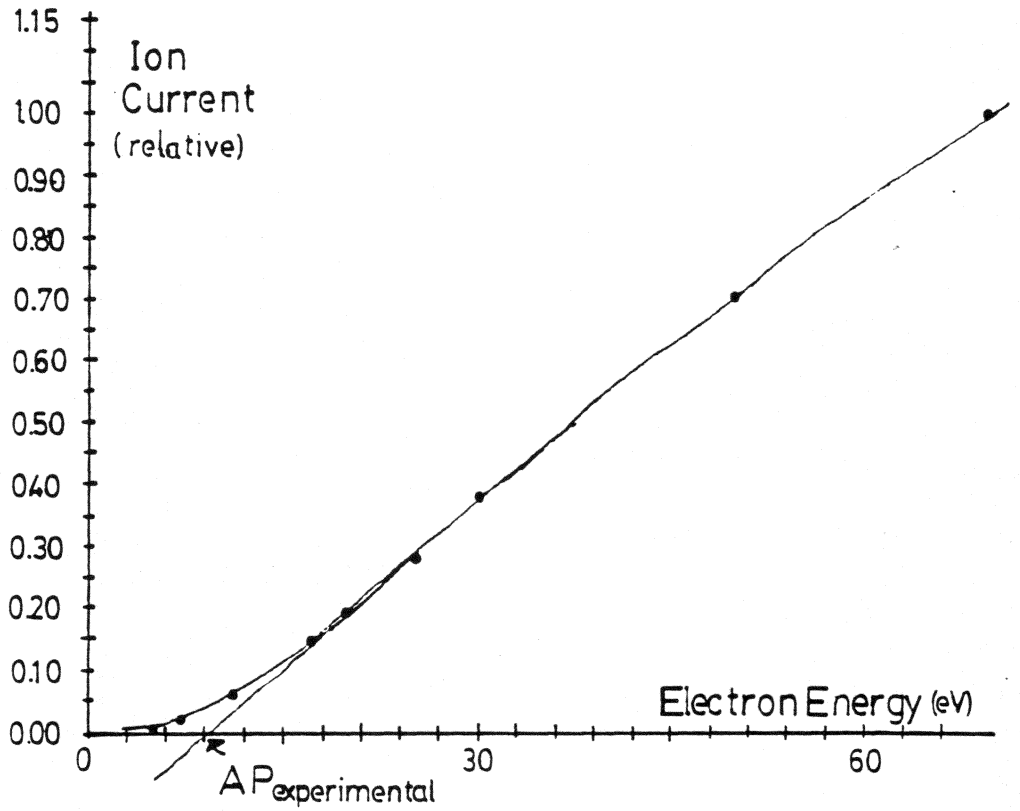

Figure 6 - Appearance Potential

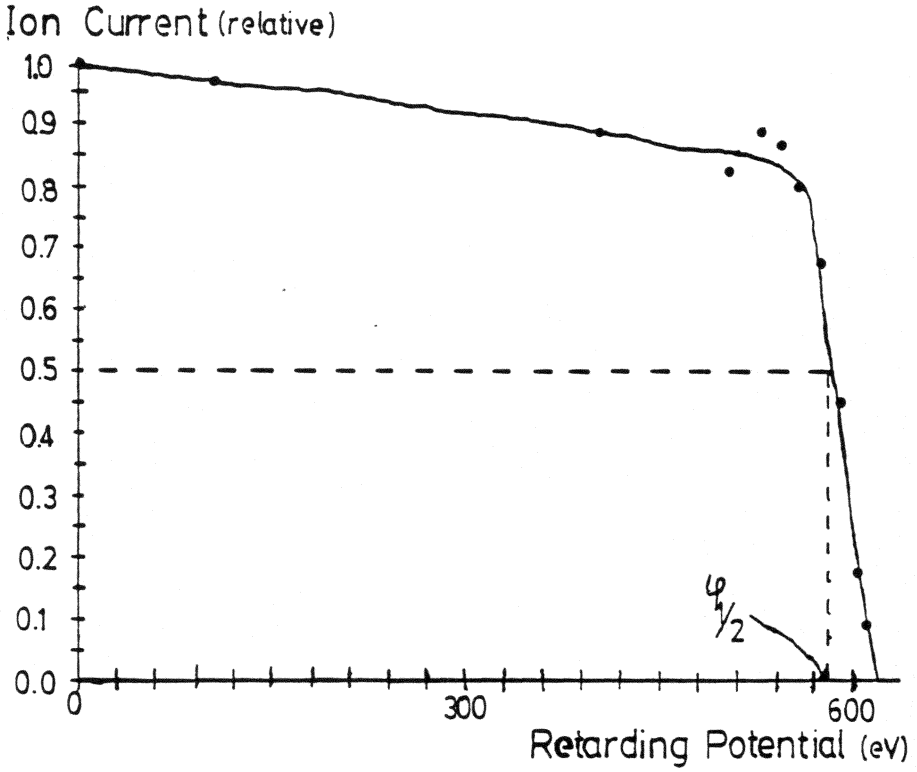

Figure 7- Ion Energy Determination

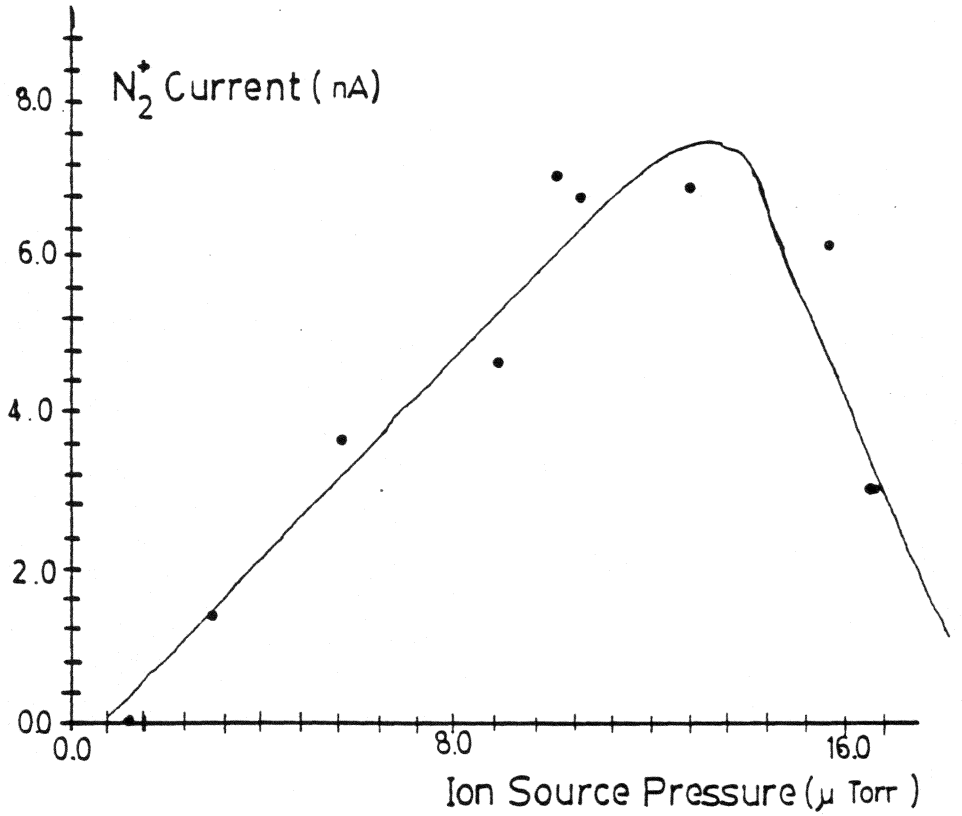

Figure 8 - Source Pressure vs. Ion Current

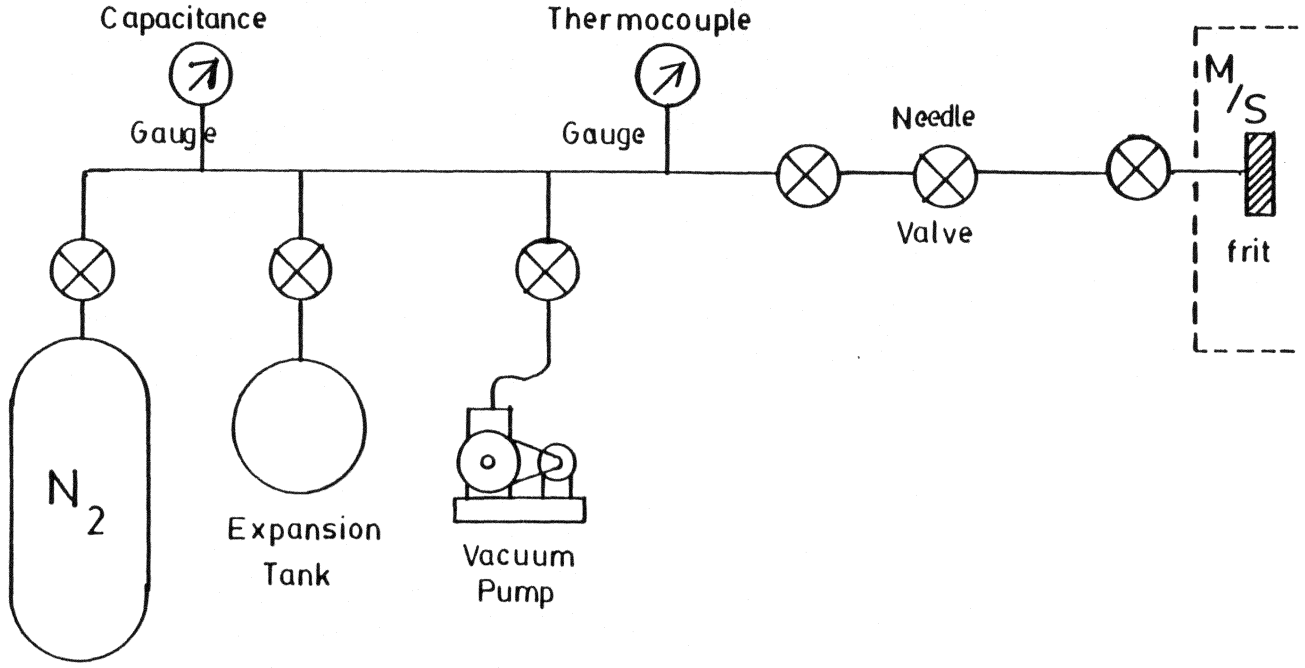

Figure 9 - Ion Source Inlet System

III C. 2) Ion Transport

The ion beam produced in the ion source must be transported to the reaction cell. The ion optics were designed to accomplish this function. The current set of ion optics (Figure 10) were designed and constructed by A. Smith[32]. They may be conveniently divided into two parts, those that reside in the chamber ("T") attached to the mass spectrometer, and those that reside in the chamber that holds the reaction cell. The first element (inside the "T") is called the Ring Drawout (RD) and acts as a mirror to redirect the ion beam toward the reaction cell. The next element (L1) is used to collimate the redirected ion beam. The remaining elements are used to provide focus and collimation. Typical operating voltages are given in Table 6. Ion currents (for N_2^+) were on the order of $1.1*10^{-9}$A at the end of the "T" and $1.9*10^{-10}$A at the exit of the ion optics. When focused to provide maximum current through the reaction cell (*i. e.* at the rear beam flag) a current of $1.3*10^{-10}$A was seen on the cell and screen and a current of $1.9*10^{-11}$A was seen at the exit of the cell. Thus the total transmission of the ion optics was on the order of 20% through the first stage (inside the "T") and 20% through the second stage for a total

transmission of about 4%. This compares quite unfavorably with the total beam current at the cell of $1.7*10^{-9}$A reported by A. Smith[32]. The exact reasons for this discrepency are still unknown. In addition to problems with low-beam-current levels, severe problems with beam stability also existed. For unknown reasons, the beam levels would drop below those necessary to perform the experiment. Attempts at cleaning, alignment, and readjustment of voltage levels were only marginally sucessful. Because the current levels could not be increased to useable levels, it was decided to reduce noise by use of a modulated detection system.

TABLE 6

Typical Values for Ion Optics

(all voltages relative to ground)

Element	Voltage
RD	+123
L1	-411
T1	+225
T2	-243
L2	0
T3	+190
FD1	+14
FD3	+39
FD2	+83
FD4	+83

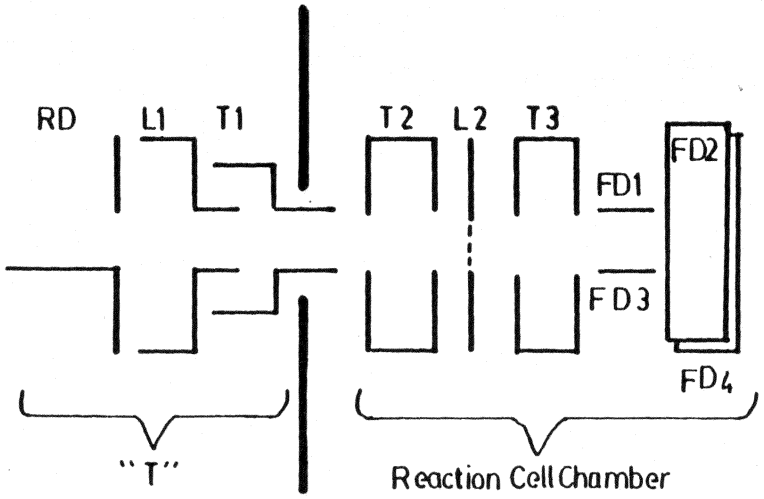

Figure 10 - Ion Optics[32] (not to scale)

III D. 3) Reaction Cell

The reaction cell (Figure 11) is the chamber in which the target gas was placed and reaction products were measured. The pressure was maintained in the 10^{-4}Torr range by the cell inlet system (Figure 12). The system was evacuated with a mechanical vacuum pump. Gas was then admitted into the small tank and expanded into the large tank with resulting pressures below 20Torr. The manifold pressure was measured accurately with a calibrated Bourdon gauge (Wallace and Tiernan model FA160 0-20Torr, readable to 0.01Torr). The gas flows into the cell through a frit of $9.74*10^{-6}ls^{-1}$ conductance.[32] The entrance and exit of the cell are copper plates with a knife-edged circular orifice of 0.110cm and 0.159cm, respectively. Since the pressure in the cell is in the molecular region, the conductance (C) can be calculated:

(48) $$C = 11428\ r^2\left[\frac{T}{m}\right]^{1/2}$$

where the conductance is in cm^3/sec, r is the radius in cm, T is the temperature in Kelvins, and m is the molecular weight in g/mole.[34] At equilibrium the flows

into and out of the cell are equal:

(49) $$P_{cell}\, C_{cell} = P_{inlet}\, C_{frit}$$

or,

(50) $$P_{cell} = \frac{P_{inlet}\, C_{frit}}{C_{cell}} \quad .$$

Thus, the pressure in the cell can be calculated from the pressure in the inlet system.

The beam flag (BF1) has a smaller (0.079cm radius) circular hole than the entrance and prevents measurement of current that does not enter the reaction cell. The exit flag (BF2) measures the current which passes through the cell without reaction or scattering. Typically, about 25 to 30% of the beam was transmitted through the cell (with gas present). This indicates a very good focus through the cell.

The product ions are produced with largely thermal kinetic energies (*i. e.* little momentum transfer exists). Because of this, it is possible to separate

scattered incident ions from product ions by energy analysis. A potential difference ($\Delta\Phi$) is applied between the screen (CTCS), which is made of mesh, and the solid reaction cell. At zero potential, some of the scattered reactant and product ions will hit the screen (because it has finite area). As the potential is increased (the cell is made more positive) the slow product ions will be attracted to the grid while the fast (scattered) ions will not be deflected enough to avoid being collected on the cell wall. Thus, a plot of I_{CTCS} / I_{TOTAL} *vs.* $\Delta\Phi$ (Figure 13) will show a minimum current at $\Delta\Phi = 0$ and will show an increase to a maximum $\left[\left|\frac{I_{CTCS}}{I_{TOT}}\right|_{\Delta\Phi \to \infty}\right]$ at a value of $\Delta\Phi \approx 20V$. The charge transfer current is given by

$$(51) \qquad I_{CT} = \left.\frac{I_{CTCS}}{I_{TOT}}\right|_{\Delta\Phi \to \infty} - \left.\frac{I_{CTCS}}{I_{TOT}}\right|_{\Delta\Phi \to \infty}$$

Upon inserting this in the equation for cross section (equation 13) the following is obtained:[32]

$$(52) \qquad \sigma = \frac{-kT}{P_{cell}\,x} \ln\left[1 - \left.\frac{I_{CTCS}}{I_{TOT}}\right|_{\Delta\Phi \to \infty} + \left.\frac{I_{CTCS}}{I_{TOT}}\right|_{\Delta\Phi = 0}\right].$$

This provides the cross section in terms of the experimentally measured variables. The measurement of ion current is covered in the next section.

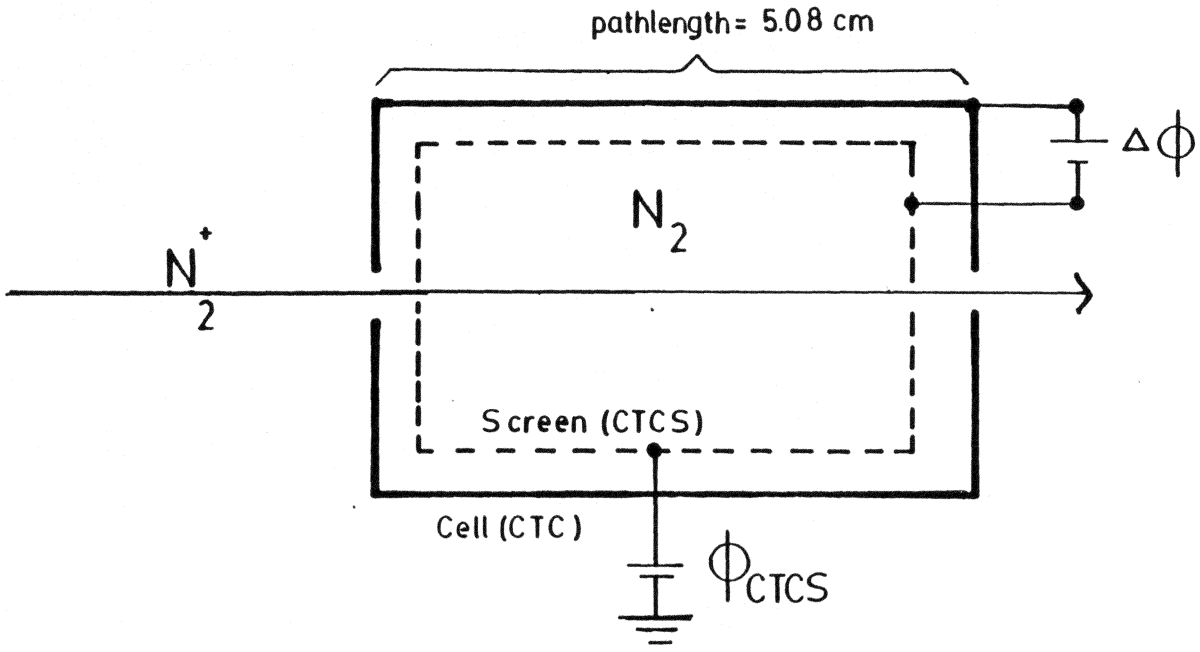

Figure 11- Charge Transfer Cell

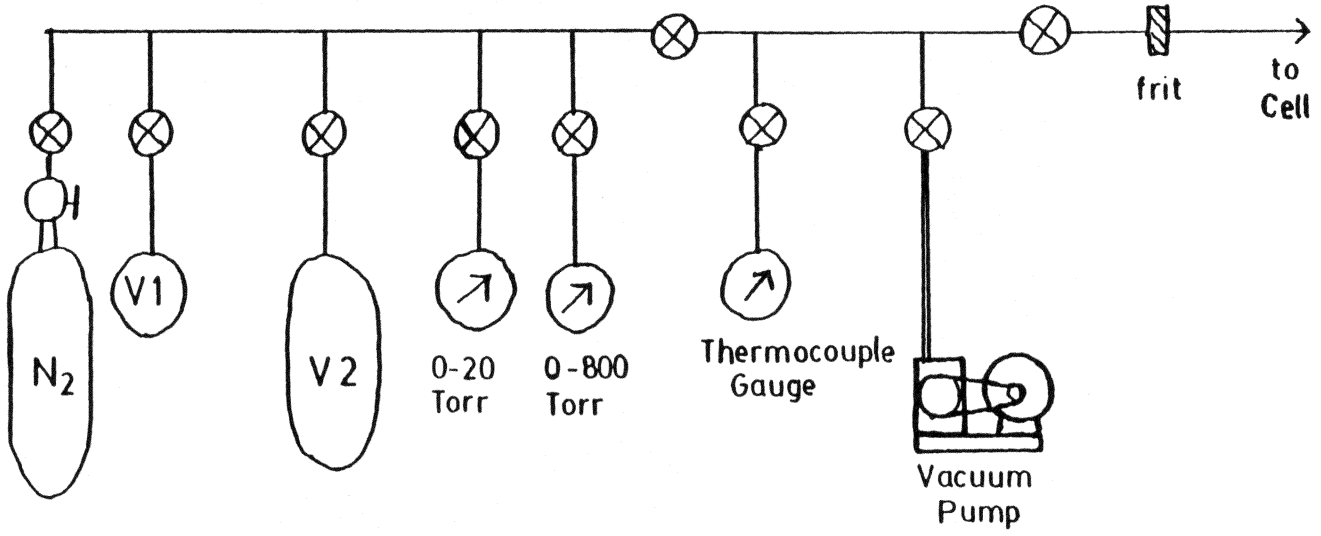

Figure 12-Cell Inlet System

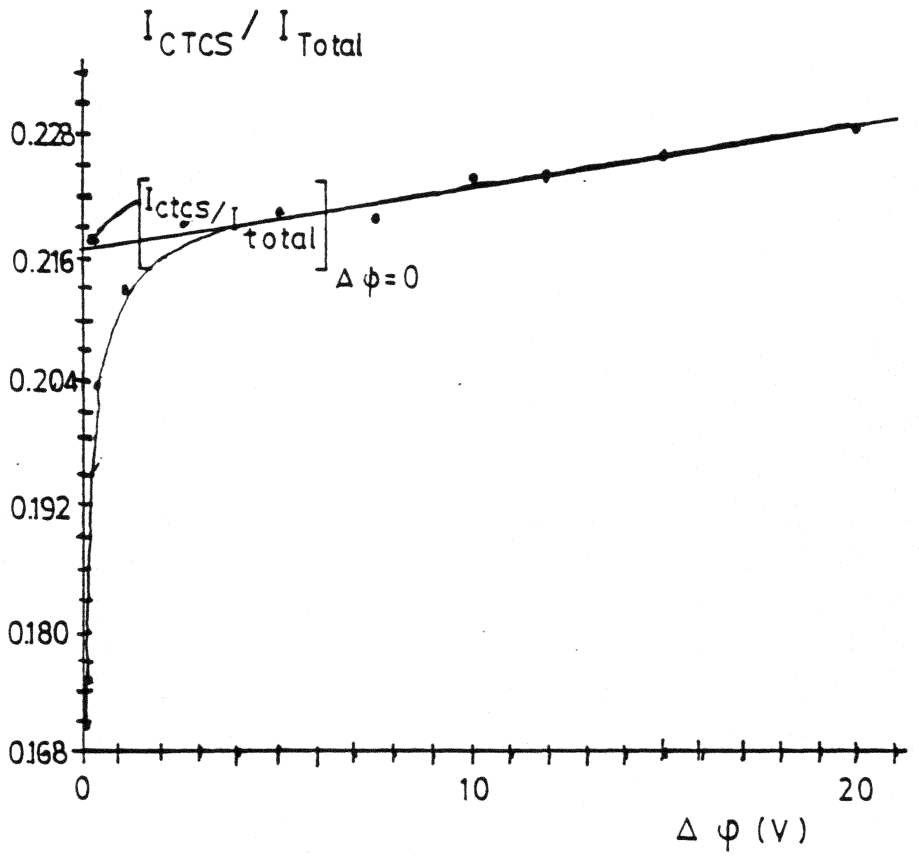

Figure 13 - Determination of Charge Transfer Current

III E. 4) ION DETECTION

Originally, measurement of ion current was made with an electrometer (Keithley model 602) which is capable of measuring currents at up to ±1500V above ground. Since only one such electrometer was available, a switching arrangement was employed (Figure 14). The switch is a ceramic-rotary-wafer switch. To reduce leakage, only every other set of poles was used. This results in a non-connected position between the CTC measure and CTCS measure positions. The switch was originally mounted in a polystyrene box with coaxial feed-throughs used for the supplies and connections to the CTC and CTCS. Unfortunately, the leakage due to the conductivity of the box made this unusable. The switch was then mounted on a 0.25in. piece of Plexiglas (TM) with the extermal connections made directly to the switch. This arrangement proved generally sucessful although extremely humid conditions still caused excessive leakage. This was partially a result of inadequate room humidity control and poor sealing of the room from outside air. Electrical leakage occured both at the ceramic switch and at the coaxial feed-throughs (used to pass the CTC and CTCS connections through the wall of the vacuum system).

Heating the surfaces with a hot-air drier did not provide any improvement. Spraying the surface with 2-propanol did reduce the leakage but required an overnight wait to allow the alcohol to evaporate (Attempts to speed drying with forced hot air were not sucessful). It is likely that the treatment with 2-proponol also removed surface oils and dirt from the surfaces.

Although coaxial feedthroughs were used for the CTC and CTCS leads, great difficulties were experienced with leakage currents. Some idea of the problem involved can be obtained by applying Ohm's law:

(53) $$R = \frac{E}{I} .$$

With a minimum current (I) on the order of $1*10^{-13}$A and a cell retarding potential (E) of 100V, the minimum resistance (R) to ground must be greater than 10^{15} Ohms. Unfortunately, the resistive current was not constant but exhibited a pronounced "spiking" tendency. This was likely due to small breakdowns in the insulation which vanish after the charge (current) has dissipated. Additional severe problems with capacitive (and possibly

piezoelectric and/or triboelectric) pickup produced noise with instrument vibration and operator movement. Because of these problems and the low level of ion beam current, it was decided to use a modulated detection system.

Modulation was applied to the element RD (in the ion-transport optics). This element was chosen because it was sensitive to voltage level. Also, it was felt that modulation applied to the ion source might affect state distribution and energy levels. A Krohn-Hite model 5800A signal generator was used with a Bogen model 0100A amplifier. They were isolated from the d.c. voltage of the RD element with a Stancor model P-6461 filament transformer ($117V_{in}$, $10V_{out}$) that was reversed to provide approximately a 10:1 step-up ratio (Figure 15). Best results were obtained with a sine wave with frequency of about 200cps (Hertz). Frequency and a.c. voltage were measured with a Hewlett-Packard model 140A oscilloscope.

Detection of signals was performed with an Applied Research model 128A lock-in amplifier. This device acts as a phase (and frequency) sensitive a.c. rms voltmeter that measures only the component of the imput at the same phase and frequency as the reference signal.

This greatly reduces noise and eliminates problems with d.c. leakage current. Since the signals to be measured were currents, while the lock-in amplifier is a voltmeter, a 4MOhm resistor was placed across the electrometer terminals. The signal to the lock-in amplifier was taken across that resistor. The amplifier has an adjustable phase network which was used to compensate for a phase shift between the modulation input and the ion signal. This shift was the same for both cell and screen electrodes. Severe problems were encountered with ground loops in the a.c. supply circuits. These were reduced by insuring a common ground point for all power supplies and floating the case ground for the supplies to the cell and screen. Although this reduced the severity of ground-loop noise to usuable levels, it did not completely eliminate noise due to ground loops. In particular, severe noise was seen each weekday from about 4:45 to 5:30 pm. The exact source is not known but is likely due to equipment shutdown on campus at end of normal office hours. Additional support for this hypothesis comes from the observation that noise levels were generally lowest during night-time hours. It should be noted that the problem with ground loops was probably no worse for detection with the lock-in amplifier than was the case for detection with

the electrometer. However, the use of an oscilloscope to monitor the output of the lock-in amplifier made detection of ground loops much easier. Additional noise was picked up from the fluorescent lamps on the ceiling above the apparatus. This necessitated the installation of incandescent lamps to be used in place of the fluorescent lamps. In spite of these difficulties, the use of modulated detection greatly improved the signal-to-noise ratio and made measurement possible at much lower signal strengths. Additionally, the use of modulation detection greatly reduced problems with humidity and other sources of d.c. leakage currents.

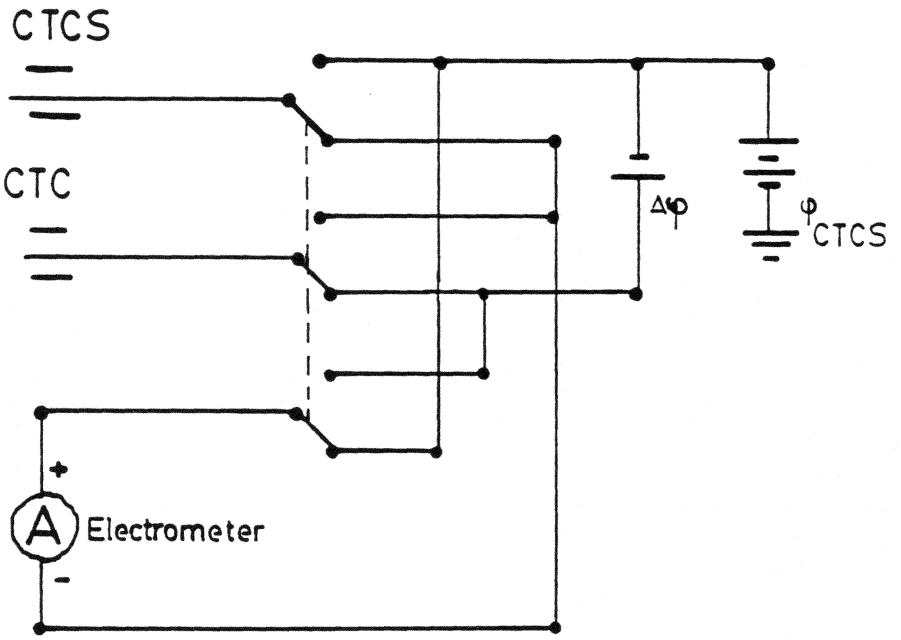

Figure 14 - Electrometer Switch

(CTCS measurement shown)

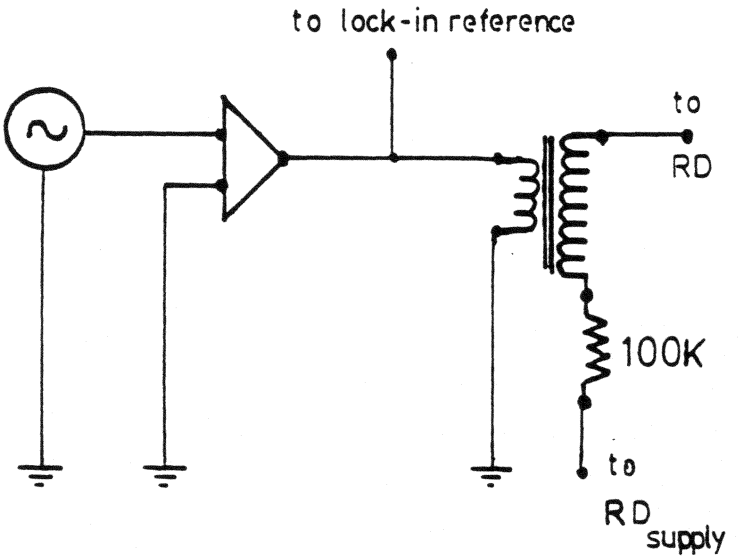

Figure 15 - Modulation Source

IV. EXPERIMENTAL RESULTS AND CONCLUSIONS

Experimental cross sections obtained with electrometer detection are presented in Table 7. Experimental cross sections with modulated detection (lock-in amplifier) are presented in Table 8. The reaction-cell pressures in both sets are similar. These pressures are toward the upper range in which cross section linearity exists[32] and were chosen in an attempt to maximize signal. As stated earlier in the section on ion optics, there were severe problems with the level of ion beam current and with intermittent instrumental failures.

The data will be reviewed with emphasis on the following questions:

1) What is the effect of electrometer versus modulated detection?

2) What is the effect of electron energy on the charge transfer cross section?

3) What is the effect of ion energy (collision velocity) on charge transfer cross section?

The first of these questions is best addressed by

noting that the use of modulated detection eliminated most problems associated with leakage currents. As noise had reached levels that prevented cross section measuremt, the use of modulated detection became essential. An additional aspect is the effect of modulated detection on precision. This was investigated by combining data at similar ion energies and then examining the variance of each set (Table 9). The F ratio test may be expressed as

$$F(n,d) \equiv \frac{V_n}{V_d}, \tag{54}$$

where F(n,d) is the value of the F ratio for n degrees of freedom in the numerator, d degrees of freedom in the denominator, and V_n and V_d are the variances of the numerator and denominator respectively. Comparing each electrometer data set to the modulated data, an F(23,18) of 1.80 is obtained for the higher energy set and F(23,20) of 10.6 is obtained for the lower energy set. The probabilities that the reduction in variance is not due to chance are 89.7% and greater than 99.99%, respectively.[35] Viewed in this manner, modulated detection is definitely seen to provide more replicable data than electrometer detection. Unfortunately, the F ratio test between the

two electrometer data sets (taken at different energies) gives a value of F(20,18) = 5.90, which is significant at greater than 99.96%.[35] Thus the reduction in variance between the data sets might also be due to increasing ion energy; the variance may be less at higher ion energies. To separate these two factors, it would be necessary to run modulated detection data sets at various ion energies (perferably the same as those by electrometer detection) and to analyze the variance. Because of instrumental difficulties, this was not completed but should be seriously considered in future work. It is likely that the variance is related to the noise present when the various data sets were run. Indeed the increase of noise that occured when the lowest energy set was run prompted the use of modulated detection. Since this noise was present even at high ion energies and was substantially reduced by modulated detection, it is felt that the precision of the cross section data was indeed improved by the use of modulated detection.

A useful analysis of precision can be obtained by considering the replicate measurements listed in Table 11 and plotted in Figure 16. The average of the 95% "Student's t" (actually Gosset's t) confidence limits is

$\pm 7.4 \text{Å}^2$ for 4 runs (3 degrees of freedom). In order to experimentally confirm an 8% dip in cross section at low electron energies, the confidence limit must be reduced to about 2Å^2. The reduction in the variance (σ^2) varies with the reciprocal of the number of measurements (n):

(55)
$$\sigma^2 = \frac{\sigma^2_{measured}}{n},$$

where $\sigma^2_{measured}$ is the measured variance. Since the confidence limit varies with the square root of the variance, the reduction in the confidence limit varies with $n^{-1/2}$. This means that some 10 to 20 times the number of measurements for each electron energy will be needed to see such a dip (unless current signal levels can be improved). To provide this degree of confidence at each of 5 electron and 5 ion energies would require on the order of 1000 to 2000 cross section measurements. Clearly either a dramatic improvement in precision or a totally automated operation would be needed to establish suitably accurate cross sections.

The second question (What is the effect of electron energy on cross section?) is addressed by fitting

a least-squares line (Figures 17, 18, and 19, and Table 10) to the cross-section-versus-electron-energy data (at fixed ion energies). The slopes and intercepts of these lines are given in Table 10. The validity of such a line may be examined by considering the reduction in variance between the zeroth and first order (linear least-squares) fits.[36] The F ratio for this reduction in variance (see Table 10) is 2.85 for the beam with 479eV ion energy, 1.05 for the beam with 226eV ion energy, and 3.69 for the beam with 59eV ion energy. These are statistically different from chance at 90.0%, 67.8%, and 93.3% respectively. Thus the relationship between electron energy and cross section at an ion energy of 226eV can not be demonstrated. This is likely due to scatter in the data. The relationship in the other two data sets, however, appears to be justified. The dependence of cross section on the electron energy leads to two important conclusions. First, the energy variation in the electron beam affects the precision of the cross section (although this effect is extreamly minor in the preset experiment). Second, and more importantly, the electron energy used to produce the ions must be accurately known if various experimental values of cross sections are to be compared. This requires regular comparison of the electron energy to accepted standards

(such as the known appearance potential of an ionic species). Because of the scatter in the data, differences in the slopes are not statistically significant and attempts to examine trends in the slope are not justified. With this reservation in mind, it is still interesting to examine the observed trend of decreasing slope and increasing intercept with decreasing ion energy. At higher electron energies it is expected that the ions would be produced in higher vibrational states. Due to the vibrational overlap factors between ion and neutral (for $N_2^+ - N_2$), the lowest vibrational states should possess the greatest cross sections. At lower ion velocities the interaction time increases and the difference between the reactivity of the vibrational states should become more marked. Further research is needed to confirm this observation.

The third question (What is the effect of ion energy on cross-section?) is addressed with the same approach as the second question addressed. Unfortunately, the large scatter in the data (relative to the effect of ion energy) made attempts to plot a trend line totally unjustified. The very small slope of such a line ($\approx 3*10^{-3} Å^2/eV$) is indicative of the ion influence of ion

energy on cross section. The fact that less dependence is seen on ion energy than on electron energy (for $N_2^+ - N_2$) emphasis the importance of having well-defined electron energies.

As an analysis of accuracy, the mean cross section at an electron energy of 78eV is plotted with cross sections of A. Smith and other workers in Figure 20.[32] An examination of Figure 20 indicates that the difference between laboratories is on the order of 3 to $5Å^2$ at high energies and about $10Å^2$ at low energies. The variation within laboratories appears to be roughly half of the difference between laboratories. This variation within laboratories is on the order of the variance experienced in this experiment. This indicates the universal difficulty of obtaining cross section values of sufficient precision and accuracy to test theoretical models and to test for trends in experimental data.

In conclusion, the previous work of A. Smith[32] demonstrated the validity of the present technique in measuring resonant-charge-exchange cross sections. However, it was felt that the previous work had uncertanities with respect to electron energy and that the

precision of the previous work could not be evaluated. The current work has shown that electron energy is a major influence on cross section for N_2 charge transfer and that a knowledge of the energy of the electron beam is necessary for comparison to values of other laboratories as well as for comparison to theoretical calculations. An analysis of the precision of the current work has shown the difficulty of obtaining sufficiently precise value of cross section to permit evaluation of experimental trends. It is felt that this difficulty is not unique to this work but is a general problem in cross section measurement. The resolution of this problem will pose a considerable challange to future work, but will be necessary for the advancement of both experimental and theoretical evaluation of charge transfer.

With regards to future work, it is suggested that the cell be placed directly at the exit of the mass spectrometer. Since commercial mass spectrometers have a well collimated beam in order to obtain high mass-resolution, it is likely that adequate collimation can be obtained by a slit in front of the charge-transfer cell. This would eliminate the ion optics, with the consequent advantages of more beam current at the cell, better reliability, and better beam stability.

TABLE 7

Cross Section Data for

$N_2^+ + N_2 \rightarrow N_2 + N_2^+$

with Electrometer Detection

Corrected Ion Energy (eV)	Corrected Electron Energy (eV)	Cross Section ($Å^2$)	Pressure $*10^{-4}$ Torr
225	76.9	27.3	1.22
225	56.9	27.9	1.22
225	47.0	30.2	1.22
225	34.8	30.6	1.22
225	37.0	24.3	1.22
234	77.5	33.4	1.22
234	57.5	30.3	1.22
234	37.5	31.5	1.22
234	33.5	29.9	1.22
234	27.5	35.2	1.21
234	25.0	31.6	1.21
234	23.5	31.8	1.21
219	80.9	13.9	1.21
219	60.9	20.0	1.21
219	40.9	25.4	1.21

Table 7 (cont.)

Cross Section Data for

$N_2^+ + N_2 \rightarrow N_2 + N_2^+$

with Electrometer Detection

Corrected Ion Energy (ev)	Corrected Electron Energy (ev)	Cross Section ($\AA^2$)	Pressure $*10^4$Torr
219	35.9	23.6	1.21
219	30.9	28.2	1.21
219	28.4	14.4	1.21
119	80.9	10.3	1.20
119	60.9	9.5	1.20
119	40.9	11.5	1.20
119	35.9	8.4	1.20
119	30.9	18.6	1.20
82	79.0	20.6	1.24
82	59.0	18.1	1.24
82	39.0	12.5	1.24
82	34.0	16.6	1.24
60	78.5	22.7	1.19
60	58.5	23.6	1.19

Table 7 (cont.)

Cross Section Data for

$N_2^+ + N_2 \rightarrow N_2 + N_2^+$

with Electrometer Detection

Corrected Ion Energy (ev)	Corrected Electron Energy (ev)	Cross Section ($\AA^2$)	Pressure $*10^4$Torr
60	38.5	31.0	1.19
60	33.5	28.0	1.19
60	28.5	36.4	1.20
60	26.0	48.9	1.19
60	23.5	36.7	1.19
56	78.2	45.6	1.25
56	38.2	29.4	1.25
56	33.2	39.0	1.25
56	28.1	37.8	1.25
56	25.7	61.8	1.25
38	80.9	19.0	1.30
38	60.9	16.6	1.30
38	40.9	38.5	1.30
38	35.9	60.2	1.30

Table 8

Cross Section Data for $N_2^+ + N_2 \rightarrow N_2 + N_2^+$

with Lock-in Amplifier Detection

Corrected Ion Energy (eV)	Corrected Electron Energy (eV)	Cross Section ($\AA^2$)	Pressure $*10^4$Torr
420	74.0	23.1	1.19
420	54.0	28.2	1.19
420	34.0	27.8	1.19
420	29.0	30.5	1.19
420	24.0	34.1	1.19
420	21.5	32.6	1.19
420	19.0	33.8	1.19
520	75.0	23.4	1.19
520	55.0	26.8	1.19
520	35.0	28.1	1.19
520	30.0	24.5	1.19
520	25.0	30.8	1.19
520	22.5	29.3	1.19
520	20.0	23.2	1.19
520	75.0	27.0	1.19
520	55.0	27.5	1.19
520	40.0	34.4	1.19
520	35.0	30.9	1.19

Table 8 (cont.)

Cross Section Data for $N_2^+ + N_2 \rightarrow N_2 + N_2^+$

with Lock-in Amplifier Detection

Corrected Ion Energy (ev)	Corrected Electron Energy (ev)	Cross Section ($Å^2$)	Pressure $*10^{-4}$ Torr
520	30.0	32.5	1.19
520	27.5	29.0	1.19
457	78.0	24.3	1.17
457	58.0	18.4	1.17
457	38.0	21.6	1.17
457	33.0	25.6	1.17
457	28.0	19.5	1.17
457	23.0	21.5	1.17
457	23.0	22.3	1.17

TABLE 9

Comparison of Precision for Cross Section Data

$$N_2^+ + N_2 \rightarrow N_2 + N_2^+$$

Method	Average Ion Energy (eV)	Cross Section ($Å^2$)	Variance $(Å^2)^2$	Degrees of Freedom
modulated	479	26.4	19.1	23
electrometer	226	27.3	34.4	18
electrometer	59	32.9	203	20

TABLE 10

Cross Section ($\AA$) versus Electron Energy (eV)

method	Ion Energy (ev)	slope ($\AA^2$/ev)	intercept ($\AA^2$)	
modulated	479	-0.077	30.1	F(1,25) = 2.85
electrometer	226	-0.080	30.8	F(1,16) = 1.05
electrometer	59	-0.291	46.4	F(1,19) = 3.69

TABLE 11

Confidence Limits for Cross Sections

(modulated detection, Ion Energy = 479eV)

(four measurements)

corrected electron energy eV	cross section ($Å^2$)	95% confidence limits ($Å^2$)
76	24.5	±2.8
56	25.2	±7.3
41	28.0	±8.3
36	28.3	±6.1
30	29.2	±10.5
27	25.2	±9.2
		average = ±7.4

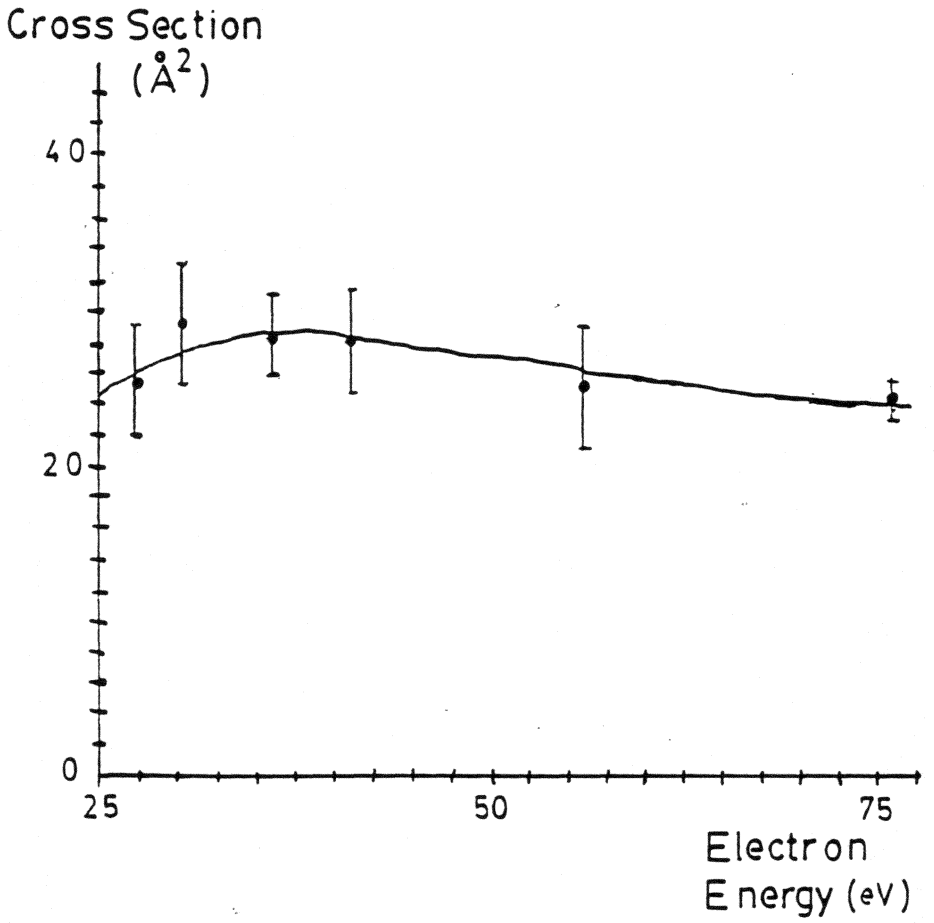

Figure 16 Cross Section for N_2 Charge Transfer
(IonEnergy = 479eV, error bar for 70 %
confidence limits)

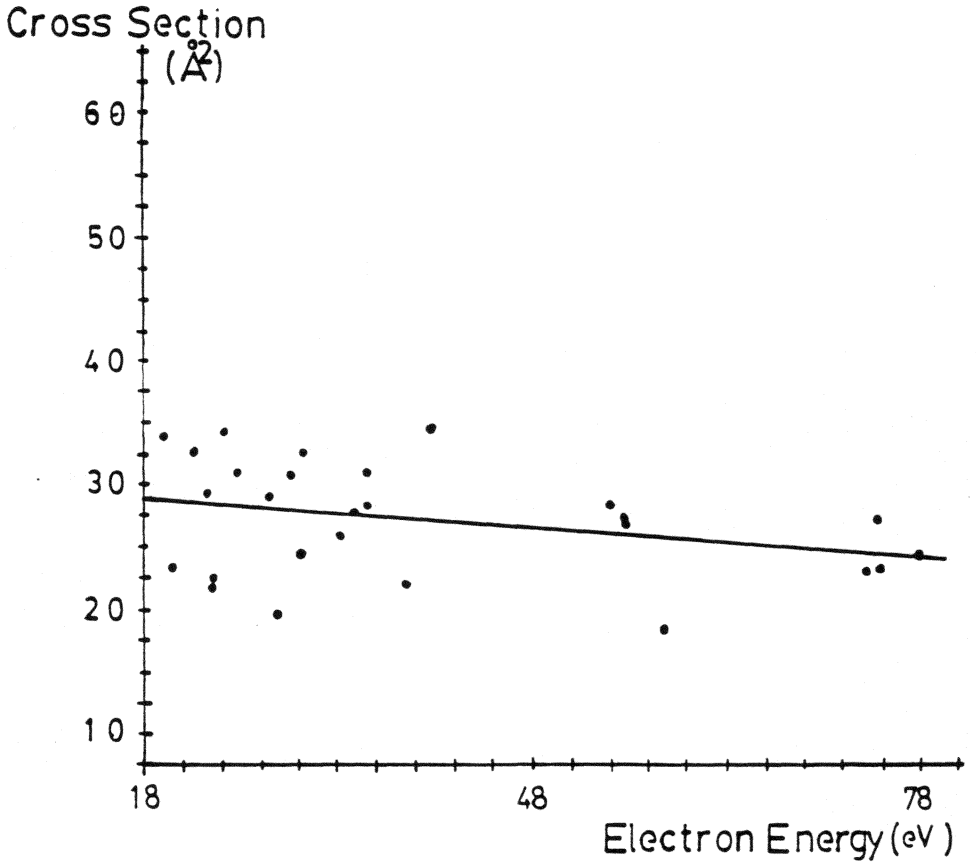

Figure 17- Cross Section for N_2 Charge Exchange (modulated detection, Ion Energy = 479 eV)

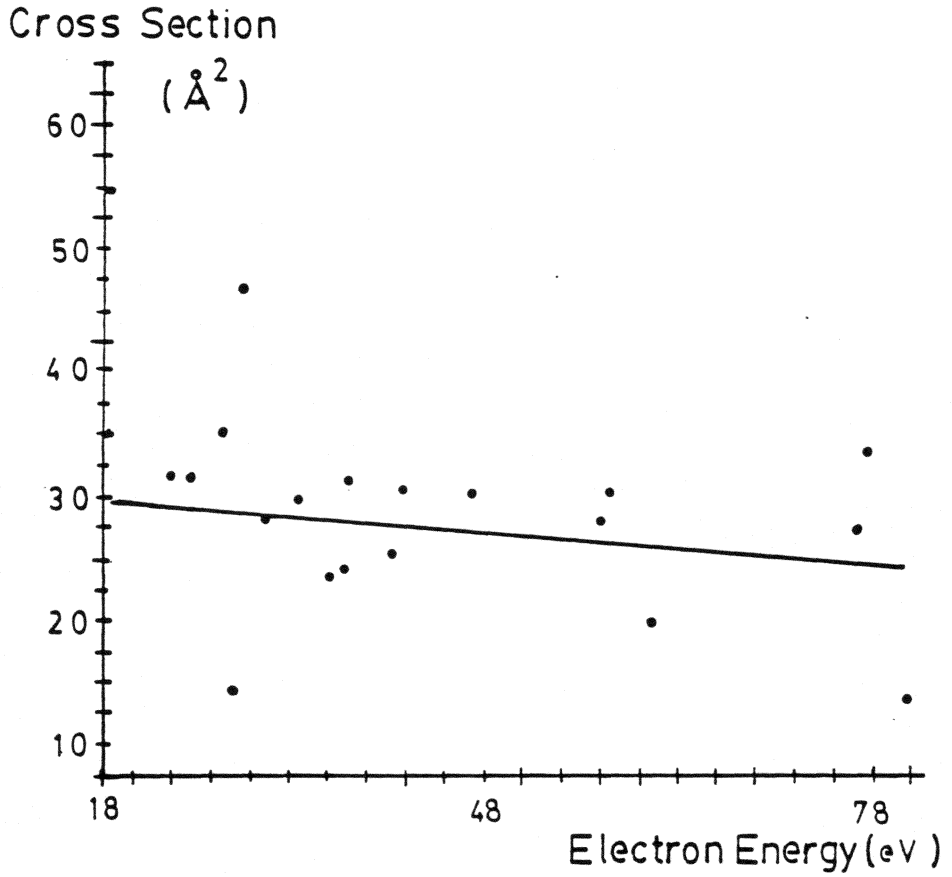

Figure 18 - Cross Section for N_2 Charge Exchange (electrometer detection, Ion Energy = 226 eV)

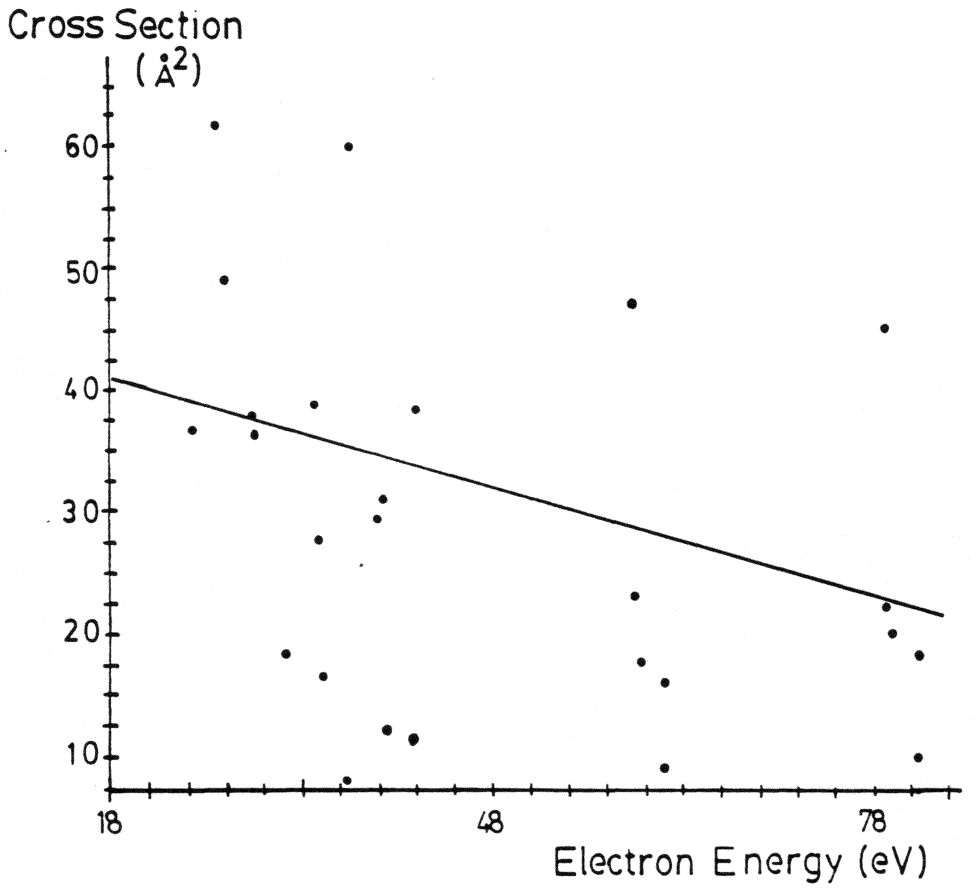

Figure 19 - Cross Section for N_2 Charge Exchange (electrometer detection, Ion Energy = 59 eV)

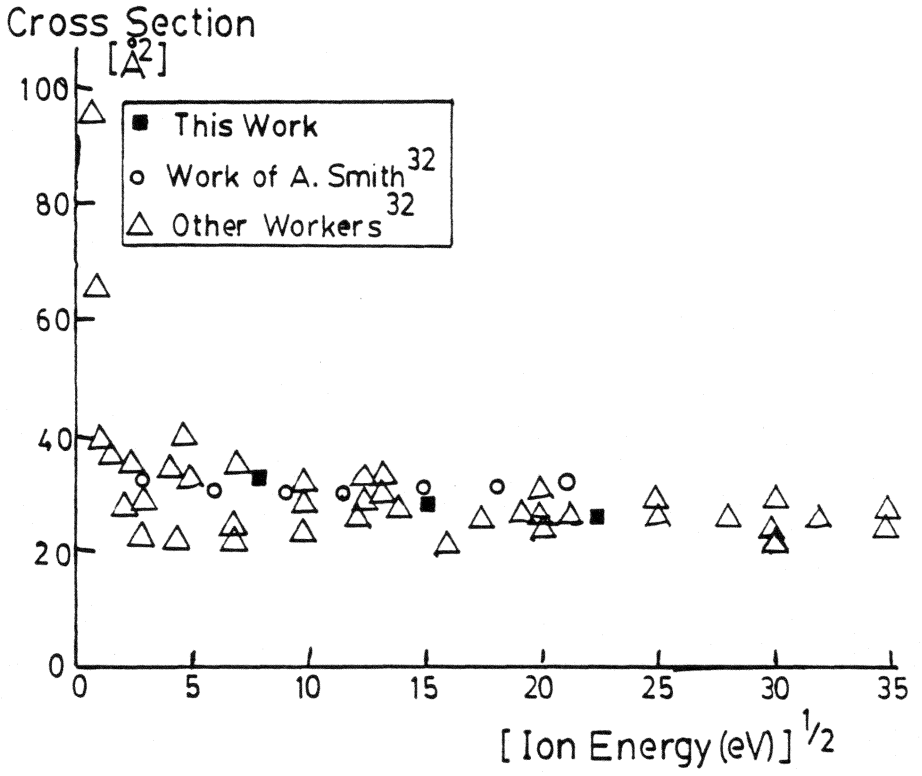

Figure 20- Comparison to Other Workers

REFERENCES

1) D. Adams, "The Hitchhiker's Guide to the Galaxy", (radio program) episode 4 (first series), British Broadcasting Co. BBC Radio 4, (1978).

2) B. Mahan and A. O'Keefe, Journal of Chemical Physics, vol.76, p. 4433 (1982).

3) J. Collin, J. Delwiche, and P. Natalis, International Journal of Mass Spectrometry and Ion Physics, vol. 7, p. 19 (1971).

4) T. F. Moran, M. R. Flannery, and P.C. Cosby, Journal of Chemical Physics, vol. 61, p. 1261 (1974).

5) Y. Kaneko, Journal of the Physical Society of Japan, vol. 16 p. 1587 (1960).

6) B. Mahan and A. O'keefe, Journal of Chemical Physics, vol. 76, p. 4433 (1982).

7) J. Allison, T. Kondow, and R. N. Zare, Chemical Physics Letters, vol. 64, p. 202 (1979).

8) F. Gilmore, Journal of Quantitative Spectroscopy and Radiative Transfer, vol. 5, p. 369 (1965).

9) M. R. Flannery, P. C. Cosby, and T. F. Moran, Journal of Chemical Physics, vol. 59, p. 5494 (1973).

10) R. F. Holland and W. B. Maier II, Journal of Chemical Physics, vol. 56, p. 5229 (1972).

11) P. Krupperie and S. Weissman, Journal of Chemical Physics, vol. 43, p. 1529 (1965).

12) J. Desequelles, M. Dufany, and M. C. Paulizac, Physics Letters A, vol. 27, p. 96 (1968).

13) A. J. Blake and J. H. Carver, Journal of Chemical Physics, vol. 48, p. 1602 (1968).
14) B. R. Turner, J. A. Rutherford, and D. M. J. Compton, Journal of Chemical Physics, vol. 48, p. 1602 (1968).

15) T. Su and M. T. Bowers in GAS PHASE ION CHEMISTRY, vol. 1, T. Su and M. T. Bowers ed.s, 1979 Academic Press, p. 83 - 118.

16) G. Gioumousis and D. P. Stevenson, Journal of Chemical Physics, vol. 29, p. 294 (1957).

17) J. J. Leventhal, T. F. Moran, and L. Friedman, Journal of Chemical Physics, vol. 46, p. 4666 (1967).

18) D. Rapp and W. E. Francis, Journal of Chemical Physics, vol. 37, p. 2631 (1962).

19) T. F. Moran and W. H. Hamill, Journal of Chemical Physics, vol. 39, p. 1413 (1963).

20) J. V. Dugan, Jr. and J. L. Magee, Journal of Chemical Physics, vol. 47, p. 3103 (1967).

21) J. O. Hirschfelder, C. F. Curtiss, and R. B. Bird, MOLECULAR THEORY OF GASES AND LIQUIDS,1964, John Wiley and Sons, New York, p. 950.

22) J. V. Dugan, Jr. and R. B. Canright, Jr., Journal of Chemical Physics, vol. 56, p. 3623 (1972).

23) R. A. Barker and D. P. Ridge, Journal of Chemical Physics, vol. 64, p. 4411 (1976).

24) E. F. Gurnee and J. L. Magee, Journal of Chemical Physics, vol. 26, p. 1237 (1957).

25) Walter J. Moore, PHYSICAL CHEMISTRY, fourth ed. (1972), Prentice Hall, Englewood Cliffs, NJ, p. 342.

26) D. R. Bates and R. H. G. Reid, Proceedings of the Royal Society, part A Vol. 310, p.1 (1969).

27) D. Rapp and W. E. Francis, Journal of Chemical Physics, vol. 37, p. 2631 (1962).

28) S. B. Sears and A. E. DePristo, Journal of Chemcal Physics, vol. 77, p. 290.

29) A. E. DePristo and S. B. Sears, Journal of Chemical Physics, vol. 77, p. 298.

30) A. J. Blake and J. H. Carver, Journal of Chemical Physics, vol. 47, p. 1038 (1967).

31) A. Maslow as quoted in Superlearning, S. Ostrander, L. Schroeder, and N. Ostrander, Dell Publishing Co., New York, (1982) p. 147.

32) A. Smith, Phd., Disseration; Virginia Polytechnic Institute and State University, Blacksburg, Va., May 1977.

33) Consolidated Engineering Corporation, Operation and Maintenance Nanual, Mass Spectrometer Model 21-401, Pasadena, Ca., Oct. 1953.

34) S. Dushman, Scientific Foundation of Vacuum Technique, John Wiley and Sons, New York, 1962, p. 92.

(35) L. Poole, M. Borchers, and K. Koessel, Some Common Basic Programs TRS-80™ Level II Edition, Osborne/McGraw - Hill, Berkeley, Ca., 1981, p. 140.

(36) J. Mandel, The Statistical Analysis of Experimental Data, Dover Publications, New York, 1984, p. 160 - 181.

The vita has been removed from the scanned document